

# 000 001 002 003 004 005 006 007 008 009 010 011 012 013 014 015 016 017 018 019 020 021 022 023 024 025 026 027 028 029 030 031 032 033 034 035 036 037 038 039 040 041 042 043 044 045 046 047 048 049 050 051 052 053 EMERGENCE OF SUPERPOSITION: UNVEILING THE TRAINING DYNAMICS OF CHAIN OF CONTINUOUS THOUGHT

006 **Anonymous authors**

007 Paper under double-blind review

## 011 ABSTRACT

013 Previous work shows that the chain of continuous thought (continuous CoT) im-  
014 proves the reasoning capability of large language models (LLMs) by enabling  
015 implicit parallel thinking, and a subsequent work provided theoretical insight by  
016 showing that a two-layer transformer equipped with continuous CoT can effi-  
017 ciently solve directed graph reachability by maintaining a superposition of mul-  
018 tiple reasoning traces in the continuous thought. However, it remains unclear  
019 how the superposition mechanism is naturally learned from gradient-based train-  
020 ing methods. To fill this gap, we theoretically analyze the training dynamics of  
021 a simplified two-layer transformer on the directed graph reachability problem to  
022 unveil how the superposition mechanism emerges during training in two training  
023 stages – (i) a *thought-generation* stage that autoregressively expands the contin-  
024 uous thought, and (ii) a *prediction* stage that converts the thought into the final  
025 answer. Our analysis reveals that during training using continuous thought, the  
026 index-matching logit, an important quantity which reflects the strength of the  
027 model’s local search ability, will first increase and then remain bounded under  
028 mild assumptions. The bounded index-matching logit effectively balances explo-  
029 ration and exploitation during the reasoning process: the model will exploit lo-  
030 cal problem structures to identify plausible search traces, and assign comparable  
031 weights to multiple such traces to explore when it is uncertain about which solu-  
032 tion is correct, which results in superposition. Our experimental results tracking  
033 the growth of logits further validate our theory.

## 035 1 INTRODUCTIONS

036  
037 Large Language Models (LLMs) show great reasoning capabilities in many complex tasks, espe-  
038 cially when equipped with chain-of-thought (CoT) (Wei et al., 2022). However, due to the large  
039 inference cost of long CoT for complex tasks, many recent works seek alternative test-time scal-  
040 ing methods to more efficiently improve LLMs’ reasoning ability (Goyal et al., 2023; Wang et al.,  
041 2023b; Pfau et al., 2024; Su et al., 2025).

042 One promising method is to use chain-of-continuous-thought (COCONUT, or continuous CoT) (Hao  
043 et al., 2024), where the reasoning trace of an LLM is kept in a continuous latent space instead of pro-  
044 jected back to the discrete token space. Continuous CoT exhibits both theoretical advantages (Zhu  
045 et al., 2025) and empirical performance gains (Hao et al., 2024) in many tasks. To more efficiently  
046 and reliably scale up continuous CoT to solve more challenging tasks, it requires a deeper under-  
047 standing of its internal mechanism.

048 Previous work (Zhu et al., 2025) theoretically shows that one of the most important advantages  
049 of continuous CoT is that it can enable the model to reason by superposition: when the model  
050 encounters multiple plausible search traces and is uncertain about which one is correct, it can keep  
051 all plausible traces in parallel since the CoT is in continuous space instead of discrete tokens. In  
052 particular, Zhu et al. (2025) abstracted a family of reasoning tasks as a directed graph reachability  
053 problem, i.e., whether there exists a path from a given start node to a given destination node, and  
showed that a two-layer transformer with  $O(n)$  (where  $n$  is the number of vertices in the graph)

054 continuous thought decoding steps can efficiently solve the task by providing a construction of the  
 055 parameters. Therefore, a natural next question is:  
 056

057 *Do gradient-based methods naturally lead to such a construction, and can we  
 058 theoretically prove it?*

059  
 060 This paper answers the above question affirmatively by theoretically analyzing the training dynamics  
 061 of a (simplified) two-layer transformer on the graph reachability problem in two training stages: (i) a  
 062 *thought generation* stage where the model autoregressively generates a chain of continuous thoughts  
 063 and (ii) a *prediction* stage where the model predicts the final answer using the generated thought.

064 Importantly, our analysis of the thought generation training stage reveals why the superposition  
 065 can *emerge* even if the training data only presents one demonstration for each training sample.  
 066 Our theoretical analysis as well as experimental results show that when training with continuous  
 067 thought (i.e., the COCONUT training method in Section 3 and Section 5), the index-matching logit,  
 068 an important quantity that measures the strength of model’s local search capability, will remain  
 069 bounded under mild conditions, which is in contrast to many previous analysis on transformer logit  
 070 without continuous thought (e.g., Tian et al. (2023a); Nichani et al. (2024a); Nguyen & Nguyen-  
 071 Tang (2025)) where the logit will grow logarithmically and thus unbounded. A bounded index-  
 072 matching logit can balance exploration and exploitation: if the logit is too small, the model cannot  
 073 even perform local search, resulting in a nearly random guess in the next step; if the logit is too large,  
 074 the model might over-confidently commit to one of the plausible search traces merely depending on  
 075 local features (e.g., the indegree of a node in our case) even if it is uncertain about the solution, and  
 076 thus early discard the correct path. A bounded index-matching logit encourages the model to exploit  
 077 the local structure while explore multiple plausible solutions by assigning comparable weights to  
 078 them, which naturally results in superposition. This answers the question of Zhu et al. (2025) why  
 079 superposition can emerge during training.

080 **1.1 RELATED WORKS**

081 **Reasoning with chain of thought.** Chain-of-thought (CoT) (Wei et al., 2022) is a simple yet  
 082 effective test time scaling method to enhance LLM’s reasoning capability. It can either be prompt-  
 083 based only (Khot et al., 2022; Zhou et al., 2022) or be included in the training sample to create  
 084 high-quality training data (Yue et al., 2023; Yu et al., 2023; Wang et al., 2023a; Shao et al., 2024).  
 085 Beyond empirical study, many theoretical works also explore the advantages of the CoT method. For  
 086 example, Liu et al. (2022); Feng et al. (2023); Merrill & Sabharwal (2023); Li et al. (2024b) shows  
 087 that CoT can improve the expressivity of transformers. Zhu et al. (2024) studies the importance of  
 088 CoT for two-hop reasoning via training dynamics. Wen et al. (2024); Kim & Suzuki (2024) studies  
 089 how CoT in the training data can improve the sample efficiency of transformers. Instead of the text-  
 090 based CoT, this paper studies continuous CoT where the “thinking tokens” lie in a latent continuous  
 091 space and do not need to be converted to discrete tokens.

092 **Latent space reasoning.** A recent line of work studies latent space reasoning, a novel paradigm  
 093 beyond text-based CoT (Goyal et al., 2023; Wang et al., 2023b; Pfau et al., 2024; Su et al., 2025; Hao  
 094 et al., 2024). For example, Goyal et al. (2023) proposed to use pause tokens, which are learnable  
 095 tokens that are inserted into the original text to increase the computation space. Later, London &  
 096 Kanade (2025) theoretically shows that the pause token can strictly increase the expressivity of the  
 097 transformer. Similarly, Pfau et al. (2024) studies filler tokens, which also increase the computation  
 098 space of LLMs. Wang et al. (2023b) proposed to use planning tokens at the beginning of the response  
 099 generation to improve the reasoning capability. Su et al. (2025) proposed to use abstract tokens in  
 100 a latent space to enhance the reasoning performance while reducing the inference cost. The most  
 101 related work is Hao et al. (2024), which proposes to use continuous CoT for reasoning. A follow-up  
 102 work Zhu et al. (2025) theoretically shows the advantage of continuous CoT via expressivity. Our  
 103 work takes a further step by analyzing the training dynamics of continuous CoT.

104 **Training dynamics of transformers.** There is a rich line of literature studying the optimization  
 105 of transformer-based models (Jelassi et al., 2022; Bietti et al., 2023; Mahankali et al., 2023; Fu  
 106 et al., 2023; Tian et al., 2023a;b; Zhang et al., 2024; Li et al., 2024a; Huang et al., 2024; Guo et al.,  
 107 2024). A line of more recent works focus on the understanding of reasoning abilities or patterns

108 of transformers via training dynamics, including the induction heads (Nichani et al., 2024a), the  
 109 reversal curse (Zhu et al., 2024), CoT (Wen et al., 2024; Kim & Suzuki, 2024), factual recall (Nichani  
 110 et al., 2024b), in context two hop reasoning (Guo et al., 2025), out of context reasoning (Huang et al.,  
 111 2025), etc. Along the line, our paper aims to understand the internal mechanism of continuous CoT  
 112 and why superposition emerges via the analysis of training dynamics.  
 113

## 2 PROBLEM FORMULATION

117 **Basic notations.** We use  $[N]$  to denote the set  $\{1, 2, \dots, N\}$  for any integer  $N > 0$  and use  $[i : j]$   
 118 to denote  $\{i, i+1, \dots, j-1, j\}$  for integers  $i \leq j$ . For any finite set  $\mathcal{X}$ , we use  $|\mathcal{X}|$  to denote its  
 119 cardinality and use  $\text{Unif}(\mathcal{X})$  to denote the uniform distribution over  $\mathcal{X}$ . We use  $\mathbb{R}$  to denote the set  
 120 of real numbers and denote  $x_+ = \max(x, 0)$  for  $x \in \mathbb{R}$ . For any vector  $\mathbf{x} = (x_1, \dots, x_d) \in \mathbb{R}^d$ , the  
 121 softmax function  $\text{SoftMax}(\cdot) : \mathbb{R}^d \rightarrow \mathbb{R}^d$  is defined as  $\text{SoftMax}(\mathbf{x})_i = \exp(x_i) / (\sum_{j=1}^d \exp(x_j))$ .  
 122 Let  $\mathbf{I}_d \in \mathbb{R}^{d \times d}$  denote the identity matrix. Let  $\text{Voc} = [M]$  denote a vocabulary of size  $M$  for a  
 123 fixed integer  $M > 0$ . For each token  $v \in \text{Voc}$ , there is an associated embedding  $\mathbf{E}(v) \in \mathbb{R}^d$ . Let  
 124  $\mathbf{U} = [\mathbf{E}(1), \mathbf{E}(2), \dots, \mathbf{E}(M)] \in \mathbb{R}^{d \times M}$  be the token embedding matrix.  
 125

126 **Graph and permutation.** For a directed graph  $\mathcal{G} = (\mathcal{V}, \mathcal{E})$  with the vertex set  $|\mathcal{V}| = n$  and  
 127 the edge set  $\mathcal{E} = \{(s_i \rightarrow t_i)\}_{i=1}^m$ , we fix a root node  $\mathbf{r} \in \mathcal{V}$  and two candidate destination  
 128 nodes  $c_1, c_2 \in \mathcal{V}$  such that exactly one node, denoted  $c_*$ , is reachable from  $\mathbf{r}$  and denote the  
 129 other as  $c_\perp$  that is unreachable. For a radius  $c \in \mathbb{N}$ , define the  $c$ -ball as  $\mathcal{N}_c^{\mathcal{G}}(\mathbf{r}) = \{v \in \mathcal{V} : v$   
 130 is reachable from  $\mathbf{r}$  within  $c$  steps}. For a subset  $\mathcal{V}' \subseteq \mathcal{V}$ , we define the restricted in-degree as  
 131  $\text{deg}_{\mathcal{G}, \mathcal{V}'}^-(v) = |\{u \in \mathcal{V}' : (u \rightarrow v) \in \mathcal{E}\}|$ . We also fix a shortest path from  $\mathbf{r}$  to  $c_*$  as  $p =$   
 132  $(p_0, \dots, p_C)$  with  $p_0 = \mathbf{r}$ ,  $p_C = c_*$ ,  $(p_{c-1} \rightarrow p_c) \in \mathcal{E}$  for any  $c \in [C]$ . For any permutation  $\pi$   
 133 over  $\mathcal{V}$ , we define  $\pi(\mathcal{G}) = (\mathcal{V}, \pi(\mathcal{E}))$ , where  $\pi(\mathcal{E}) = \{(\pi(s) \rightarrow \pi(t)) \mid (s \rightarrow t) \in \mathcal{E}\}$ , and define  
 134  $\pi(p) = (\pi(p_0), \dots, \pi(p_C))$ . We also denote the set of all permutations over  $\mathcal{V}$  as  $S_{\mathcal{V}}$ .  
 135

136 **Chain of continuous thought.** Let  $\text{TF}_\theta(\cdot) : (\mathbb{R}^d)^* \rightarrow \mathbb{R}^d$  be a transformer which receives an  
 137 input embedding sequence  $\mathbf{h} = \mathbf{h}_{[t]} \triangleq (\mathbf{h}_1, \mathbf{h}_2, \dots, \mathbf{h}_t) \in \mathbb{R}^{d \times t}$  and outputs  $\text{TF}_\theta(\mathbf{h}) \in \mathbb{R}^d$ . For  
 138 convenience, we assume weight tying. A traditional decoder using a discrete CoT will sample the  
 139 next token  $v_{t+1} \sim \text{SoftMax}(\mathbf{U}^\top \text{TF}_\theta(\mathbf{h}))$ . Then the embedding of  $v_{t+1}$  will be appended to the  
 140 end of the input, i.e.,  $\mathbf{h}_{t+1} = \mathbf{E}(v_{t+1})$ . For continuous CoT, one directly appends the output of the  
 141 transformer to the end of the input sequence without converting it to a token, i.e., setting  $\mathbf{h}_{t+1} =$   
 142  $\text{TF}_\theta(\mathbf{h})$ . Assume the prompt  $\mathbf{x} = [x_1, \dots, x_{t_0}] \in \text{Voc}^{t_0}$  and its corresponding embedding sequence  
 143 is  $\mathbf{h}_{[t_0]} = [\mathbf{h}_1, \dots, \mathbf{h}_{t_0}] = [\mathbf{E}(x_1), \dots, \mathbf{E}(x_{t_0})]$ . For notation convenience, we use  $[\mathbf{t}_c] = \mathbf{h}_{[t_0+c]}$   
 144 to denote the continuous thought generated at decoding step  $c$ , where  $[\mathbf{t}_c] = \text{TF}_\theta(\mathbf{h}_{[t_0+c-1]})$ .  
 145 In particular,  $[\mathbf{t}_0] = \mathbf{h}_{t_0}$ . After  $C$  decoding steps, one can append a special token  $\langle \text{A} \rangle$  at the  
 146 end of the sequence to trigger the transformer to switch the mode and generate the final answer.  
 147 Specifically, one can set  $\mathbf{h}_T = \mathbf{E}(\langle \text{A} \rangle)$  where  $T = t_0 + C + 1$  and generate the final answer  
 148  $\widetilde{\text{TF}}_{\theta, C, \mathbf{U}}(\mathbf{h}_{[t_0]}) := \arg \max_{v \in \text{Voc}} \mathbf{U}^\top \text{TF}_\theta(\mathbf{h}_{[T]})$ .  
 149

150 **Graph reachability and prompt format.** In this paper, we mainly focus on the directed graph  
 151 reachability problem as studied in Zhu et al. (2025), where we are given a graph  $\mathcal{G} = (\mathcal{V}, \mathcal{E})$ , two  
 152 candidate destination nodes  $c_1$  and  $c_2$ , and a root node  $\mathbf{r}$ . The task is to identify which of the two  
 153 nodes can be reached by  $\mathbf{r}$  (denoted as  $c_*$ ). The prompt structure is illustrated in Figure 1 following  
 154 Zhu et al. (2025). The prompt consists of (1) a BOS (beginning of sentence) token  $\langle \text{s} \rangle$ ; (2) the  
 155 graph description part, which contains  $m$  edges where each edge is represented by a source node  
 156  $s_i$ , a target node  $t_i$ , and a special edge token  $\langle \text{e} \rangle$ ; (3) the task description part that contains a  
 157 special question token  $\langle \text{Q} \rangle$ , two candidate destination nodes  $c_1$  and  $c_2$ , a special reasoning token  
 158  $\langle \text{R} \rangle$  and a root node  $\mathbf{r}$ . See Table 1 for the full list of token notations. Note that  $t_0 = 3m + 6$  is the  
 159 prompt length, and let  $\mathbf{h}_{[t_0]} = (\mathbf{h}_1, \mathbf{h}_2, \dots, \mathbf{h}_{t_0})$  be the input embedding sequence. Following Zhu  
 160 et al. (2025), we use  $\text{Idx}(v)$  to denote the position of a token in the input sequence (e.g.,  $\text{Idx}(\langle \text{s} \rangle) =$   
 161 1,  $\text{Idx}(s_i) = 3i - 1$ ,  $\text{Idx}(c_1) = 3m + 3$ ,  $\text{Idx}(\langle \text{R} \rangle) = 3m + 5$ ), use  $\text{Idx}(\langle \text{e} \rangle, i) = 3i + 1$  to denote the  
 162 position of the  $i$ -th  $\langle \text{e} \rangle$  token, and use  $\text{Idx}([\mathbf{t}_i]) = t_0 + i$  to denote the position of the continuous  
 163 thought at step  $i$ . See Table 2 for the complete list of position indices.

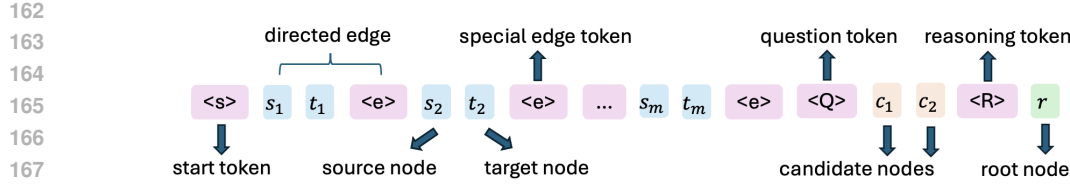
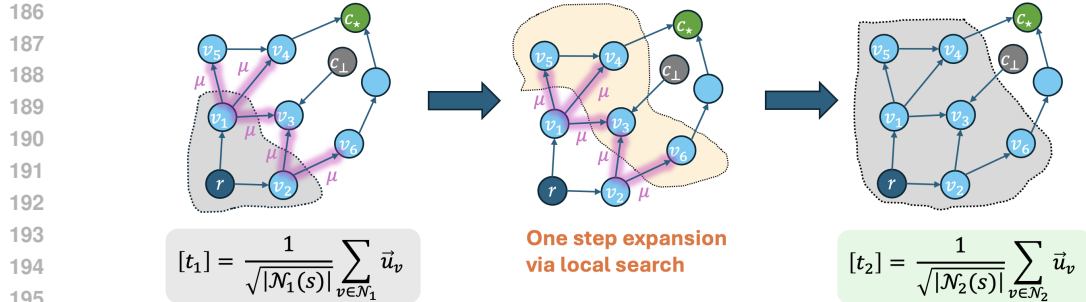


Figure 1: Prompt format of the graph reachability problem (Figure 1 of Zhu et al. (2025)).

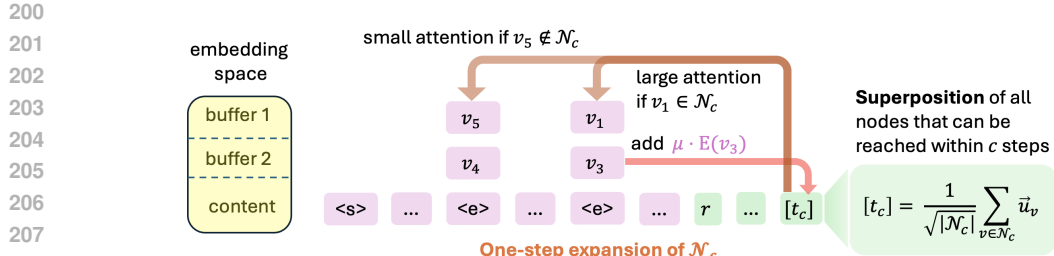
Zhu et al. (2025) provided a construction of transformer parameters  $\theta$  such that  $\widetilde{\text{TF}}_{\theta, C, \mathbf{U}}(\mathbf{h}_{[t_0]}) = c_*$  (i.e., the transformer can predict the reachable candidate node using continuous CoT) for any graph and root-candidate node tuples, where  $\mathbf{h}_{[t_0]}$  corresponds to the prompt of the graph and task descriptions. However, they did not theoretically study whether the constructed solution can be naturally learned via gradient-based methods. In the following sections, we theoretically show that the solution can be learned via gradient flow in both the thought generation stage (Section 3) and the prediction stage (Section 4). We also provide empirical results showing that the training dynamics in our theoretical analysis align well with the experiments (Section 5).

## 2.1 INDEX-MATCHING LOGITS AND LOCAL SEARCH CAPABILITY

Before we delve into the technical details in the following sections, we first provide an intuitive explanation of the dynamics of the main mechanism.



(a) **Left:** The continuous thought at step 1 [ $t_1$ ] encodes embeddings of nodes that are reachable from the root node  $r$  within one step. **Middle:** One-step expansion via local search where the strength is quantified by index-matching logit  $\mu$ . **Right:** After one-step expansion, the continuous thought at step 2 [ $t_2$ ] encodes nodes reachable within two steps.



(b) Illustration of how one-step expansion is implemented (adapted from Figure 3 of Zhu et al. (2025)). In the first layer of the transformer, each special edge token  $<e>$  copies its corresponding source and target nodes to its buffer spaces. In the second layer, as illustrated in the figure, the current thought  $[t_c]$  pays large attention to an edge if its source node has been explored, and adds its target node to the superposition, where the strength of the added node is controlled by the index-matching logit  $\mu$ . The two edges  $v_5 \rightarrow v_4$  and  $v_1 \rightarrow v_3$  corresponds to edges in Figure 2a.

Figure 2: Pictorial illustration of the superposition mechanism and the index-matching logit  $\mu$ .

216 **Global planning vs. local search.** In the context of graph reachability, the global planning refers  
 217 to a model’s capability to analyze the structure of the whole graph and then determine a path from  
 218 the root node to the destination node. In contrast, local search focuses only on which nodes are  
 219 reachable in one step from the current node, which is much easier to learn than global planning.  
 220 When using discrete CoT, the model can choose only one path at a time. Therefore, the model  
 221 needs global planning to select the correct path or to backtrack from the wrong one. When using  
 222 continuous CoT, the model can keep multiple plausible paths simultaneously. Therefore, the model  
 223 can rely solely on local search to perform parallel BFS, solving the task with only simple skills.

224 **Index-matching logits.** We use the index-matching logit  $\mu$  to quantify the strength of the model’s  
 225 local search capability, which is illustrated in Figure 2 and will be formally defined in (3) in Sec-  
 226 tion 3. In Theorem 1, we will prove that under mild conditions, the index-matching logit  $\mu$  will  
 227 first increase and then remain bounded. Note that a positive, bounded logit  $\mu$  effectively balances  
 228 exploration and exploitation in node expansion: if  $\mu$  is too small, each edge will receive similar  
 229 attention in Figure 2b, and thus the model even lacks the local search capability to exploit the local  
 230 graph structure; if  $\mu$  is too large, the model will put too much weights on nodes with large in-degree  
 231 (e.g., in Figure 2a,  $v_3$  weights  $2\mu$  and other frontier nodes such as  $v_4$  weights  $\mu$ , where the difference  
 232 in weights will be significant under large  $\mu$  and commonly used softmax attention) and thus lacks  
 233 exploration of different plausible paths.

### 235 3 ANALYSIS OF THE THOUGHT GENERATION STAGE

236 In this section, we analyze the training dynamics of the thought generation stage. We consider  
 237 any graph  $\mathcal{G} = (\mathcal{V}, \mathcal{E})$ , a root node  $r \in \mathcal{V}$ , two candidate destination nodes  $c_1, c_2 \in \mathcal{V}$ , where  
 238  $\{c_1, c_2\} \in \{c_*, c_\perp\}$  with  $c_*$  reachable from  $r$  and  $c_\perp$  unreachable. We are also given a (discrete)  
 239 CoT demonstration, which is a shortest path  $p = (p_0, \dots, p_C)$  from  $r$  to  $c_*$  where  $p_0 = r, p_C = c_*$ .

240 We use curriculum learning following Hao et al. (2024); Zhu et al. (2025), where at stage  $(c + 1)$   
 241 for any  $0 \leq c < C$ , upon receiving the prompt embeddings  $\mathbf{h}_{[c_0]}$ , the model will first generate  $c$   
 242 continuous thoughts  $[t_1], \dots, [t_c]$  autoregressively without supervision (i.e., no loss calculated  
 243 on the first  $c$  continuous thoughts at stage  $c + 1$ ), and then be trained to generate the next continuous  
 244 thought  $[t_{c+1}] = \text{TF}_\theta(\mathbf{h}_{[t_0+c]})$ . Since the learning procedure at each stage is similar, we focus  
 245 below on a fixed  $c$ .

246 Zhu et al. (2025) constructs a solution for a two-layer transformer, where the first layer mainly  
 247 performs copy (e.g., the  $i$ -th special edge token  $\langle e \rangle$  will copy the information of its corresponding  
 248 source node  $s_i$  and target node  $t_i$ ). Since the copy mechanism has been widely studied (Nguyen  
 249 & Nguyen-Tang, 2025), as well as its formation via training dynamics (Nichani et al., 2024a), we  
 250 mainly focus on the dynamics after the copy mechanism has been established. Thus, we analyze the  
 251 dynamics of the second layer of the transformer.

252 In particular, let the hidden states of each special edge token  $\langle e \rangle$  and the current thought  $[t_c]$  after  
 253 the first transformer layer be

$$254 \mathbf{h}_{\text{Idx}(\langle e \rangle, i)} = \mathbf{E}_s(s_i) + \mathbf{E}_t(t_i) \in \mathbb{R}^d, \quad \mathbf{h}_{\text{Idx}([t_c])} = \sum_{v \in \mathcal{N}_c^{\mathcal{G}}(r)} \frac{1}{\sqrt{|\mathcal{N}_c^{\mathcal{G}}(r)|}} \mathbf{E}(v) \in \mathbb{R}^d, \quad (1)$$

255 where  $\mathbf{E}_s(v) \in \mathbb{R}^d$  and  $\mathbf{E}_t(v) \in \mathbb{R}^d$  map token  $v \in \text{Voc}$  to different subspaces of  $\mathbb{R}^d$ . For example,  
 256 as in the construction of Zhu et al. (2025), we can set  $d = 3M$ , and  $\mathbf{E}_s(\cdot), \mathbf{E}_t(\cdot)$  and  $\mathbf{E}(\cdot)$  each  
 257 corresponds to  $M$  different non-zero entries. This is also similar to previous work Chen et al.  
 258 (2025); Nguyen & Nguyen-Tang (2025) where  $\mathbf{E}_s(\cdot)$  and  $\mathbf{E}_t(\cdot)$  can be viewed as previous token  
 259 heads. We make the following assumptions on the embedding  $\mathbf{E}_s(\cdot), \mathbf{E}_t(\cdot)$  and  $\mathbf{E}(\cdot)$ :

260 **Assumption 1** (Orthonormal embeddings). *Assume  $\mathbf{E}_t(\cdot) \equiv \mathbf{E}(\cdot)$ . For any  $u, v \in \text{Voc}$ ,  
 261  $\mathbf{E}_s(u)^\top \mathbf{E}_s(v) = \mathbf{E}_t(u)^\top \mathbf{E}_t(v) = \mathbb{1}\{u = v\}$  and  $\mathbf{E}_s(u)^\top \mathbf{E}_t(v) = 0$ .*

262 (1) means after the first layer, each special edge token  $\langle e \rangle$  will copy the embeddings of its  
 263 corresponding source and target nodes  $s_i$  and  $t_i$  to the same position in different subspaces. Also, we  
 264 assume by induction that after training stages  $1, 2, \dots, c$ , the current thought generated by the well-  
 265 trained model  $\mathbf{h}_{\text{Idx}([t_c])}$  is a normalized superposition of token embeddings of all nodes reachable  
 266 from  $r$  within  $c$  steps. Below, we study the training dynamics of the current stage (i.e., stage  $c + 1$ ).

270 **The forward path and reparameterization.** We consider the setting where the second layer is  
 271 attention-only. The forward pass can be formulated as  
 272

$$\begin{aligned} 273 \quad \phi(\mathbf{h}; \{\mathbf{h}_i\}_i) &= \sum_i \mathbf{V} \sigma(\mathbf{h}^\top \mathbf{W} \mathbf{h}_i) \mathbf{h}_i, \\ 274 \quad \boldsymbol{\xi} &= \mathbf{U}^\top (\mathbf{h}_{\text{Idx}([\mathbf{t}_c])} + \phi(\mathbf{h}_{\text{Idx}([\mathbf{t}_c])}; \{\mathbf{h}_{\text{Idx}(<\mathbf{e}>, i)}\}_{i=1}^m)) \in \mathbb{R}^M, \end{aligned} \quad (2)$$

275 where  $\mathbf{V}, \mathbf{W} \in \mathbb{R}^{d \times d}$  are attention parameters and  $\sigma(\cdot) : \mathbb{R} \rightarrow \mathbb{R}$  is an activation function that  
 276 determines the range of attention scores, and  $\boldsymbol{\xi} = (\xi_v)_{v \in \mathcal{V}_{\text{loc}}} \in \mathbb{R}^M$  is the output logit vector for each  
 277 token in the vocabulary. Similar to the analysis in Nguyen & Nguyen-Tang (2025), we adopt the  
 278 linear attention  $\sigma(\mathbf{h}^\top \mathbf{W} \mathbf{h}_i) = \mathbf{h}^\top \mathbf{W} \mathbf{h}_i$ , fix  $\mathbf{V} = \mathbf{I}$  and use the *index-matching* reparameterization  
 279

$$280 \quad \mathbf{W} = \sum_{v \in \mathcal{V}} \mu_v \mathbf{E}(v) \mathbf{E}_s(v)^\top, \quad \mu_v(t) = 0 \text{ for } t = 0. \quad (3)$$

281 **Remark 1.** Note that a more general form of the attention weight matrix can be  
 282

$$283 \quad \mathbf{W} = \mu_{<\mathbf{R}>} \mathbf{E}(<\mathbf{R}>) \mathbf{E}(<\mathbf{R}>)^T + \sum_{v, v' \in \mathcal{V}} \mu_{v, v'} \mathbf{E}(v) \mathbf{E}_s(v')^\top. \quad (4)$$

286 The first term only takes effect in the prediction stage (Section 4), so we can set  $\mu_{<\mathbf{R}>} = 0$  for now.  
 287 The second term involves  $n \times n$  cross terms. The symmetry of the vertices, which can be enforced  
 288 by permuting vertex labels during training, makes the  $n \times n$  parameters  $\{\mu_{v, v'}\}_{v, v'}$  effectively two  
 289 parameters  $\{\mu_1, \mu_2\}$  where  $\mu_{v, v} \equiv \mu_1$  and  $\mu_{v, v'} \equiv \mu_2$  for  $v \neq v'$ . Moreover, if we focus on the  
 290 relative value between  $\mu_1$  and  $\mu_2$ , we can further simplify the attention weight matrix by assuming  
 291  $\mu_2 = 0$ .

292 For notation simplicity, we use  $\mathbf{h}_i$  to denote  $\mathbf{h}_{\text{Idx}(<\mathbf{e}>, i)}$ , use  $\mathbf{h}_{[\mathbf{t}_c]}$  to denote  $\mathbf{h}_{\text{Idx}([\mathbf{t}_c])}$  and use  $\mathcal{N}_c$ ,  
 293  $\mathcal{N}_{c+1}$  to denote  $\mathcal{N}_c^G(\mathbf{r})$ ,  $\mathcal{N}_{c+1}^G(\mathbf{r})$ , respectively when the graph  $\mathcal{G}$  and root node  $\mathbf{r}$  is clear from the  
 294 context. We also denote  $d_u := \deg_{\mathcal{G}, \mathcal{N}_c}^-(u)$  which is the indegree of  $u$  with source nodes restricted  
 295 in  $\mathcal{N}_c$ . Finally, we denote  $K = |\mathcal{N}_c|$  and  $\lambda = \frac{1}{\sqrt{K}}$ .  
 296

297 **Loss functions.** An ideal model should be able to directly output the shortest path from the start  
 298 node  $\mathbf{r}$  to the desired candidate destination node  $\mathbf{c}_*$ , i.e., the prediction of the  $(c+1)$ -th continuous  
 299 thought  $[\mathbf{t}_{c+1}]$  exactly corresponds to the  $(c+1)$ -th step of the shortest path  $p_{c+1}$ . However,  
 300 experiments in Zhu et al. (2025) show that even for a 12-layer transformer, it is hard to predict the  
 301 shortest path even if the length of the shortest path is only 3 or 4. Therefore, we take a step back  
 302 and pursue a more practical goal – we expect the model to at least be able to generate an arbitrary  
 303 path starting from the start node  $\mathbf{r}$ , which only requires local search ability that is much easier than  
 304 the global planning ability. In the context of continuous thought, we expect the model to include  
 305 information of all vertices that are reachable from  $\mathbf{r}$  within  $(c+1)$  steps in the generated thought  
 306  $[\mathbf{t}_{c+1}]$ . We consider the following two loss functions:  
 307

$$\mathbf{COCONUT\text{-}BFS:} \quad \ell_{\mathcal{G}, \mathbf{r}}^{\text{BFS}} := -\log \frac{\sum_{v \in \mathcal{N}_{c+1}} \exp(\xi_v)}{\sum_{v \in \mathcal{V}} \exp(\xi_v)}, \quad (5)$$

$$\mathbf{COCONUT:} \quad \ell_{\mathcal{G}, \mathbf{r}, p}^{\text{coco}} := -\log \frac{\exp(\xi_{p_{c+1}})}{\sum_{v \in \mathcal{V}} \exp(\xi_v)}, \quad (6)$$

312 with permutation-averaged dataset losses  
 313

$$\mathcal{L}^{\text{BFS}} = \mathbb{E}_{\pi \sim \text{Unif}(\mathcal{S}_{\mathcal{V}})} [\ell_{\pi(\mathcal{G}), \pi(\mathbf{r})}^{\text{BFS}}] \quad \text{and} \quad \mathcal{L}^{\text{coco}} = \mathbb{E}_{\pi \sim \text{Unif}(\mathcal{S}_{\mathcal{V}})} [\ell_{\pi(\mathcal{G}), \pi(\mathbf{r}), \pi(p)}^{\text{coco}}].$$

315 Note that, intuitively, the permutation-averaged loss will lead to similar behavior across different  
 316 parameters. The first loss  $\mathcal{L}^{\text{BFS}}$  explicitly encourages the model to predict any nodes in  $\mathcal{N}_{c+1}$ .  
 317 However, in practice, it is costly and even impossible to search over the entire solution space ex-  
 318 haustively; instead, we usually present only one demonstration for each task instance during training  
 319 (in our setting, only one path  $p$  per instance  $(\mathcal{G}, \mathbf{r}, \mathbf{c}_1, \mathbf{c}_2)$ ), which corresponds to the second loss  
 320  $\mathcal{L}^{\text{coco}}$  and aligns with the practical setting where chain of thought data can be used for supervision.

321 Zhu et al. (2025) observed in experiments that superposition emerges even without explicit guid-  
 322 ance during training, i.e., using the loss  $\mathcal{L}^{\text{coco}}$ . In this paper, we investigate the emergence of  
 323 superposition by analyzing its training dynamics. The following lemma gives the gradient of the  
 324 index-matching strength parameter  $\mu_v(t)$  using gradient flow under the loss function  $\mathcal{L}^{\text{coco}}$ .

324 **Lemma 1** (Gradient of  $\mu_v$  under  $\mathcal{L}^{\text{coco}}$ ; informal version of Theorem 4 in Appendix B). *Under*  
 325 *permutation-averaged training from symmetric initialization and gradient flow*  $\dot{\mu}_v = -\alpha \nabla_{\mu_v} \mathcal{L}^{\text{coco}}$ ,  
 326 *we have*  $\mu_v(t) \equiv \mu(t)$  *for all*  $v$  *and times*  $t$ , *and the gradient of*  $\mu_v$  *is*

$$328 \quad \dot{\mu}(t) = \frac{\alpha}{n\sqrt{K}} \left( d_{p_{c+1}} - F(\mu(t)) \right), \quad F(\mu) = \frac{\sum_{u \in \mathcal{N}_{c+1}} d_u e^{\lambda(\mathbb{1}\{u \in \mathcal{N}_c\} + \mu d_u)}}{\sum_{u \in \mathcal{N}_{c+1}} e^{\lambda(\mathbb{1}\{u \in \mathcal{N}_c\} + \mu d_u)} + (n - |\mathcal{N}_{c+1}|)}.$$

330 *Moreover*  $F$  *is smooth, strictly increasing, with*  $F(-\infty) = 0$ ,  $F(+\infty) = \max_{v \in \mathcal{V}} d_v$  *and*  $0 < F(\mu) < \max_{v \in \mathcal{V}} d_v$  *for all finite*  $\mu$ .

333 The proof is deferred to Appendix B. Note that as long as  $d_{p_{c+1}} \neq \max_{v \in \mathcal{V}} d_v$ ,  $\mu(t)$  will converge  
 334 to  $\mu_* < \infty$ . In contrast, under COCONUT-BFS with loss  $\mathcal{L}^{\text{BFS}}$ ,  $\mu(t)$  will diverge to infinity. We  
 335 formalize the comparison into the following theorem and defer the proof to Appendix B.

337 **Theorem 1** (Bounded vs. divergent attention logits under COCONUT vs. COCONUT-BFS; informal  
 338 version of Theorem 4 & Lemma 5 in Appendix B). *Let*  $d_* := d_{p_{c+1}}$  *and*  $d_{\max} := \max_v d_v$ .

339 (i) *Under COCONUT-BFS (5),  $\mu(t)$  grows at least logarithmically in  $t$ , leading to unbounded*  
 340 *attention logits.*

341 (ii) *Under COCONUT (6), if  $d_* < d_{\max}$  then  $\mu(t) \rightarrow \mu^* < \infty$ , so all attention logits remain*  
 342 *uniformly bounded. If  $d_* = d_{\max}$ , then  $\mu(t) \rightarrow \infty$  at least in a logarithmic rate.*

344 **Emergence of Superposition via Bounded Attention Logits.** By Theorem 1, as long as  $F(0) <$   
 345  $d_{p_{c+1}} < d_{\max}$ , we have  $\mu(t) \rightarrow \mu^* > 0$ . Compared to many previous work (Tian et al., 2023a;  
 346 Nichani et al., 2024a; Nguyen & Nguyen-Tang, 2025) that analyze the dynamics of attention logits  
 347 in “discrete” settings where the attention logits diverge to infinity, the COCONUT training method  
 348 in continuous setting usually result in bounded attention logits. The bounded attention logits lead  
 349 to a more smooth probability distribution over next tokens, which is beneficial especially under  
 350 uncertainty: when the model is uncertain about the next step, a more smooth probability distribution  
 351 under continuous CoT mechanism results in a superposition of different plausible next steps, which  
 352 implements an effective exploration; on the contrary, an unbounded logit will result in a one-hot-like  
 353 distribution and thus the model will over-confidently commit to a plausible branch and is likely to  
 354 discard the ground-truth branch even when the evidence is weak.

355 Finally, we show that with a positive value of  $\mu$ , the continuous thought  $[t_{c+1}]$  implements a one-  
 356 step expansion from  $\mathcal{N}_c$  to  $\mathcal{N}_{c+1}$  for any graph  $\mathcal{G}$  and root node  $\mathbf{r}$ .

357 **Theorem 2** (One-step frontier expansion; informal version of Theorem 5 in Appendix B). *For*  
 358 *any graph*  $\mathcal{G}$  *and root node*  $\mathbf{r}$ , *if the current thought is any positive superposition on*  $\mathcal{N}_c^{\mathcal{G}}(\mathbf{r})$ , *i.e.,*  
 359  $[t_c] = \sum_{u \in \mathcal{N}_c} \lambda_u \mathbf{e}(u)$  *with*  $\lambda_u > 0$ , *then the next thought*  $[t_{c+1}]$  *satisfies that its token-*  
 360 *projected output*  $\mathbf{U}^{\top} [t_{c+1}]$  *is supported on the one-step expansion*  $\mathcal{N}_{c+1}$  *and has strictly positive*  
 361 *mass on every node in*  $\mathcal{N}_{c+1}$  *if*  $\mu > 0$ . *In particular,*

$$363 \quad \mathbf{U}^{\top} [t_{c+1}] = \sum_{v \in \mathcal{N}_{c+1}} \beta_v \mathbf{e}_v$$

365 *with*

$$366 \quad \beta_v = \underbrace{\lambda_v \mathbb{1}\{v \in \mathcal{N}_c\}}_{\text{carryover}} + \underbrace{\mu \sum_{u \in \mathcal{N}_c} \lambda_u \mathbb{1}\{(u \rightarrow v) \in \mathcal{E}\}}_{\text{one-hop expansion}} \geq 0.$$

370 The proof is deferred to Appendix B. Note that at initialization where  $\mu = 0$ , we have  $\beta_v = 0$  for  
 371  $v \in \mathcal{N}_{c+1} \setminus \mathcal{N}_c$ . This means every node outside  $\mathcal{N}_c$  has the same attention logits and thus the same  
 372 next token probability. However, such an exploration is not an effective exploration since it blindly  
 373 puts the same weight on almost every node in the graph without exploiting the graph structure.  
 374 Therefore, an appropriate  $\mu^* > 0$  effectively balances the exploration and exploitation: (1) it has a  
 375 positive value so the model can exploit the graph structure and can distinguish nodes within the one-  
 376 step expansion set; (2) it has a bounded value so it will not overconfidently commit to a plausible  
 377 branch while discarding other branches merely relying on local structure (such as the indegree of  
 the node) without global planning.

378 **4 ANALYSIS OF THE PREDICTION STAGE**  
 379

380 In this section, we study how the transformer learns to make the correct prediction  $c_*$  among  
 381  $\{c_1, c_2\}$  by utilizing the generated continuous thought. Note that according to Section 3, the model  
 382 is able to generate  $[t_C] = \sum_{v \in \mathcal{N}_C} \lambda_v E(v)$  with  $\lambda_v \in (0, 1]$ , a superposition of all reachable nodes  
 383 within  $C$  steps, via a balanced exploration and exploitation. We denote  $\lambda = \{\lambda_v\}_{v \in \mathcal{V}}$ . At the final  
 384 stage, one appends a special answer token  $\langle A \rangle$  at the end of the continuous CoT, i.e.,  $\mathbf{h}_T = \mathbf{h}_{\langle A \rangle}$ ,  
 385 and make the final prediction  $\text{TF}_{\theta, C, \mathbf{U}}(\mathbf{h}_{[t_0]}) := \arg \max_{v \in \mathcal{V}_{\text{oc}}} \mathbf{U}^\top \text{TF}_\theta(\mathbf{h}_{[T]})$ .  
 386

387 **The forward path and reparameterization.** Similar to (2), we formulate the forward pass in the  
 388 prediction stage as

389 
$$\phi(\mathbf{h}; \{\mathbf{h}_i\}_i) = \sum_i \mathbf{V} \sigma(\mathbf{h}^\top \mathbf{W} \mathbf{h}_i) \mathbf{h}_i, \quad (7)$$
  
 390 
$$\xi = \mathbf{U}^\top (\mu_{\langle A \rangle} \mathbf{h}_{\text{Idx}(\langle A \rangle)} + \phi(\mathbf{h}_{\text{Idx}(\langle A \rangle)}; \{\mathbf{h}_{\langle R \rangle}\})) \in \mathbb{R}^M,$$
  
 391

392 where

393 
$$\mathbf{h}_{\text{Idx}(\langle R \rangle)} = E(\langle R \rangle) + E(c_1) + E(c_2), \quad \mathbf{h}_{\text{Idx}(\langle A \rangle)} = \mathbf{h}_{[t_C]} + E(\langle A \rangle).$$
  
 394

395 Note that after the first transformer layer, the hidden state of  $\langle R \rangle$  contains information of two candidate  
 396 nodes  $c_1$  and  $c_2$  and the hidden state of  $\langle A \rangle$  contains the representation of the last thought  
 397  $[t_C]$  both due to the copy mechanism in the first layer. Again, we adopt the linear attention  
 398  $\sigma(\mathbf{h}^\top \mathbf{W} \mathbf{h}_i) = \mathbf{h}^\top \mathbf{W} \mathbf{h}_i$ , fix  $\mathbf{V} = \mathbf{I}$  and use the reparameterization

399 
$$\mathbf{W} = \mu_{\langle R \rangle} E(\langle A \rangle) E(\langle R \rangle)^\top. \quad (8)$$
  
 400

401 **Remark 2.** The scalar  $\mu_{\langle R \rangle}$  denotes the attention logit strength from  $\langle A \rangle$  to  $\langle R \rangle$ . The scalar  $\mu_{\langle A \rangle}$   
 402 represents the signal strength of the residual stream from the first layer. Also, note that the repara-  
 403 parameterization of  $\mathbf{W}$  in the prediction stage has a different form from (3) in the thought generation  
 404 stage. One can either view both (3) and (8) as special cases of a more general version (4) in or-  
 405 thogonal subspaces, or view them as two different attention heads (a thought generation head and a  
 406 prediction head).

407 **The loss function.** In the prediction stage, the goal of the model is to predict the reachable candidate  
 408 node  $c_*$ , and thus the loss function can be written as

409 
$$\ell_{\mathcal{G}, r, c_1, c_2, \lambda}^{\text{pred}} := -\log \frac{\exp(\xi_{c_*})}{\sum_{v \in \mathcal{V}} \exp(\xi_v)}, \quad \mathcal{L}^{\text{pred}} = \mathbb{E}_{(\mathcal{G}, r, c_1, c_2, \lambda) \sim \mathcal{D}} [\ell_{\mathcal{G}, r, c_1, c_2, \lambda}^{\text{pred}}], \quad (9)$$
  
 410

411 where the  $\mathcal{D} = \{(\mathcal{G}^{(i)}, r^{(i)}, c_1^{(i)}, c_2^{(i)}, \lambda^{(i)})\}_i$  denote the training set. The following lemma provides  
 412 closed-form logits for each vertex where the proof is deferred to Appendix C.

413 **Lemma 2** (Closed-form logits; informal version of Lemma 8 in Appendix C). *The logit of each  
 414 vertex  $v \in \mathcal{V}$  has the form*

415 
$$\xi_v = \underbrace{\mu_{\langle A \rangle} \lambda_v \mathbb{1}\{v \in \mathcal{N}_C\}}_{\text{residual carryover}} + \underbrace{\mu_{\langle R \rangle} \mathbb{1}\{v \in \{c_1, c_2\}\}}_{\text{candidate lift}}.$$
  
 416

417 According to Lemma 2, only the candidate node  $c_*$  has both positive residual carryover and can-  
 418 didate lift, and an appropriate relative growth rate of  $\mu_{\langle R \rangle}$  and  $\mu_{\langle A \rangle}$  ensures that  $c_*$  has the largest  
 419 logit. We formalize the result in the following theorem with proof in Appendix C.

420 **Theorem 3** (Prediction of the reachable candidate node; informal version of Theorem 6 in Ap-  
 421 pendix C). *Denote  $\mu_A = \mu_{\langle A \rangle}$  and  $\mu_R = \mu_{\langle R \rangle}$ . Let  $(\mu_{\langle A \rangle}(t), \mu_{\langle R \rangle}(t))$  follow gradient flow on loss  
 422 defined in (9). Suppose*

423 
$$\lambda_* := \min_i \lambda_{c_*}^{(i)} \in (0, 1], \quad \Delta_{\text{train}} := \max_i \max_{v \in \mathcal{N}_C^{(i)} \setminus \{c_*^{(i)}\}} (\lambda_v^{(i)} - \lambda_{c_*}^{(i)})_+ \in [0, 1].$$
  
 424

425 *Then we have*

426 
$$\frac{(\mu_A(t), \mu_R(t))}{\|(\mu_A(t), \mu_R(t))\|} \rightarrow u^*, \quad \|(\mu_A(t), \mu_R(t))\| \rightarrow \infty,$$
  
 427

432 with  $u_R^*/u_A^* = \lambda_* + \Delta_{\text{train}}$ , and  $u_R^*, u_A^* > 0$ . Consequently, for any unseen instance  
 433  $(\mathcal{G}, \mathbf{r}, c_1, c_2, \boldsymbol{\lambda})$  satisfying  $\lambda_v \in (0, 1]$  on  $\mathcal{N}_C$  and 0 otherwise, and  $\max_v \lambda_v - \lambda_{c_*} \leq \Delta_{\text{train}}$ ,  
 434 it holds that:

$$436 \quad p_{c_*}(t) := \frac{\exp(\xi_{c_*}(\mu_A(t), \mu_R(t)))}{\sum_v \exp(\xi_v(\mu_A(t), \mu_R(t)))} \xrightarrow{t \rightarrow \infty} 1.$$

## 439 5 EXPERIMENTS

441 In this section, we present experimental results validating the theoretical analysis. We first describe  
 442 the setup and overall results, then analyze training dynamics in the thought generation and answer  
 443 prediction stages.

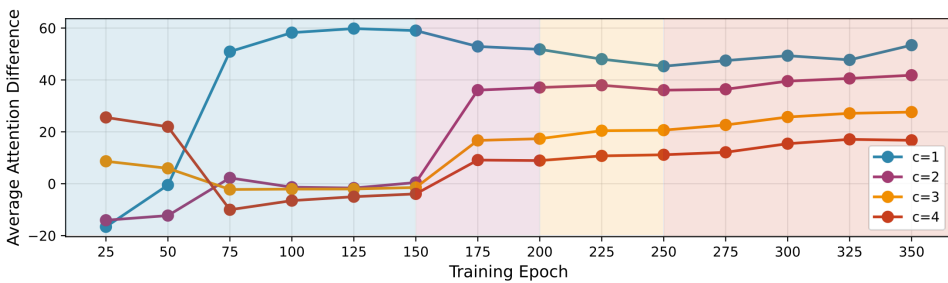
445 **Model.** We adopt a GPT-2 style decoder with two transformer layers ( $d_{\text{model}}=768$ ,  $n_{\text{heads}}=8$ ). The  
 446 model is trained from scratch with AdamW ( $\beta_1=0.9$ ,  $\beta_2=0.95$ , weight decay  $10^{-2}$ ), a constant  
 447 learning rate of  $1 \times 10^{-4}$ , and a global batch size of 256.

449 **Dataset.** We follow the dataset from Zhu et al. (2025), which is a subset of ProsQA (Hao et al.,  
 450 2024). Different from Zhu et al. (2025), we randomly permute the vertex indices in both training  
 451 and testing to avoid prediction bias and validate the symmetry assumption in (4). Dataset statistics  
 452 are summarized in Table 3.

454 **Training.** Following Hao et al. (2024); Zhu et al. (2025), we use a multi-stage training strategy  
 455 with supervision from chain-of-thought demonstrations. At stage  $c$ , the model learns to use  $c$  continuous  
 456 thoughts before predicting the  $c$ -th node on the reasoning path (*thought-generation* stage).  
 457 If  $c > l$  (the CoT length), the model predicts the final answer after  $l$  continuous thoughts and the  
 458  $\langle \mathbf{A} \rangle$  token (*prediction* stage). We train for 150 epochs at Stage 1 and 25 epochs for each subsequent  
 459 stage, totaling 350 epochs. At each stage, data from earlier stages is mixed in with probability 0.1,  
 460 which prevents the model from forgetting abilities learned from previous stages. The final accuracy  
 461 of this model on the test set is 96.2%.

### 462 5.1 THOUGHT GENERATION

464 To examine the training dynamics of  $\mu_v$  under  $\mathcal{L}^{\text{coco}}$ , we track the second-layer attention logits.  
 465 When generating the  $c$ -th continuous thought,  $\mu_v$  corresponds to the logit on an edge token  $\langle \mathbf{e} \rangle$   
 466 whose source lies in  $\mathcal{N}_c$ . In practice,  $\mathcal{L}^{\text{coco}}$  encourages the model to predict the current search  
 467 frontier rather than revisiting explored nodes, so most attention concentrates on *frontier edges*, i.e.,  
 468 edges with sources in  $\mathcal{N}_c \setminus \mathcal{N}_{c-1}$ . For theoretical simplicity, we assume  $\mu_2 = 0$  in (4). In practice,  
 469 however, the model does assign non-zero attention logits to other edges. Therefore, we report the  
 470 logit difference between frontier and non-frontier edges on the test set, which more faithfully reflects  
 471 the effective value of  $\mu_v$ .



482 Figure 3: The attention logits difference between frontier edges and others under  $\mathcal{L}^{\text{coco}}$  as a proxy for  $\mu_v$ . The  
 483 background colors indicate different training stages.

484 Figure 3 shows the results. In Stage 1 (blue background), the model gradually learns to attend to  
 485 frontier edges when predicting the first continuous thought ( $c = 1$ ). The logit difference increases

486 steadily and saturates around 60 after  $\sim 125$  epochs. This matches the theoretical prediction in  
 487 Theorem 1: under  $\mathcal{L}^{\text{coco}}$ ,  $\mu_v$  first grows and then stabilizes at a bounded value.  
 488

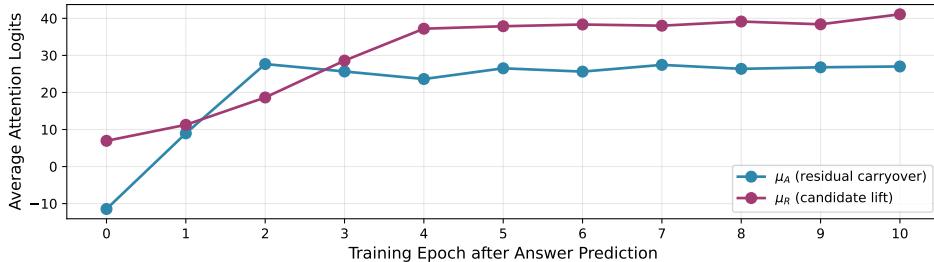
489 When switching to Stage 2 (purple background), the model requires far fewer epochs to establish  
 490 a positive  $\mu$  for  $c = 2$ . Moreover, this pattern generalizes to  $c = 3$  and  $c = 4$ , even though the  
 491 model was never explicitly trained to generate more than two continuous thoughts. This “length  
 492 generalization” indicates that once superposition emerges in earlier stages, later stages can quickly  
 493 reuse it to expand the frontier further.

494 We also trained with a variant of  $\mathcal{L}^{\text{BFS}}$ . Compared to  $\mathcal{L}^{\text{coco}}$ , the attention logit difference when  
 495  $c = 1$  did not saturate but kept increasing to much higher values, consistent with the analysis in  
 496 Theorem 1. Detailed experiments and plots are provided in Appendix E.2.

## 497 5.2 ANSWER PREDICTION

498 We next analyze how the model predicts the final answer. According to Lemma 2, the prediction  
 499 relies on two signals. The first is the *residual carryover*, which brings the explored nodes in the last  
 500 thought  $[\mathbf{t}_c]$  into the answer token with strength  $\mu_A$ . Concretely, this corresponds to the first-layer  
 501 attention from  $\langle \mathbf{A} \rangle$  to  $[\mathbf{t}_c]$ , which copies the superposition of reachable nodes. The second is the  
 502 *candidate lift*, which raises the logits of the two candidate nodes with strength  $\mu_R$ . Since  $\langle \mathbf{R} \rangle$  copies  
 503 the candidate nodes in the first layer, the second-layer attention from  $\langle \mathbf{A} \rangle$  to  $\langle \mathbf{R} \rangle$  serves as a proxy  
 504 for  $\mu_R$ .<sup>1</sup>

505 Figure 4 shows the dynamics of these two proxies. Once training enters the *prediction* stage, both  
 506  $\mu_A$  and  $\mu_R$  increase rapidly and stabilize after roughly 5 epochs. This observation is consistent  
 507 with Theorem 3, which states that  $\mu_A$  and  $\mu_R$  grow at comparable rates, ensuring that the reachable  
 508 candidate  $c^*$  attains the highest logit. In contrast to the unbounded growth predicted in theory, we  
 509 observe the logits plateau in practice. A possible reason is that, in practice, prediction-stage training  
 510 also interacts with thought generation, whereas the theory assumes fixed thought distributions to  
 511 focus on the relationship between  $\mu_R$  and  $\mu_A$ . We leave a more detailed analysis to future work.  
 512



523 Figure 4: Training dynamics of the proxies for  $\mu_A$  (residual carryover) and  $\mu_R$  (candidate lift).  
 524

## 525 6 CONCLUSIONS

526 In this paper, we study the emergence of superposition when training with continuous CoT. In par-  
 527 ticular, we theoretically analyze the training dynamics of a simplified two-layer transformer on the  
 528 directed graph reachability problem. Our analysis shows that under mild assumptions, the index-  
 529 matching logit, an important quantity showing the strength of the model’s local search ability, re-  
 530 mains bounded during training. A bounded index-matching logit effectively balances exploration  
 531 and exploitation during the reasoning process and thus enables implicit parallel thinking, which nat-  
 532 urally results in superposition. Our experimental results, which track the growth of logits, further  
 533 validate our theory. We expect our theoretical analysis to bring new insights into a deeper under-  
 534 standing of the mechanism of continuous CoT and ultimately scaling up this promising paradigm  
 535 more efficiently and reliably.

536  
 537  
 538  
 539 <sup>1</sup>We observe that under different experimental settings and random seeds, the *candidate lift* effect is not  
 always mediated by the  $\langle \mathbf{R} \rangle$  token; alternative attention routes are presented in the Appendix E.3.

540 REFERENCES  
541

542 Alberto Bietti, Vivien Cabannes, Diane Bouchacourt, Herve Jegou, and Leon Bottou. Birth of a  
543 transformer: A memory viewpoint. *Advances in Neural Information Processing Systems*, 36:  
544 1560–1588, 2023.

545 Lei Chen, Joan Bruna, and Alberto Bietti. Distributional associations vs in-context reasoning: A  
546 study of feed-forward and attention layers. In *The Thirteenth International Conference on Learn-*  
547 *ing Representations*, 2025.

548 Guhao Feng, Bohang Zhang, Yuntian Gu, Haotian Ye, Di He, and Liwei Wang. Towards revealing  
549 the mystery behind chain of thought: a theoretical perspective. *Advances in Neural Information*  
550 *Processing Systems*, 36:70757–70798, 2023.

552 Hengyu Fu, Tianyu Guo, Yu Bai, and Song Mei. What can a single attention layer learn? a  
553 study through the random features lens. *Advances in Neural Information Processing Systems*,  
554 36:11912–11951, 2023.

556 Sachin Goyal, Ziwei Ji, Ankit Singh Rawat, Aditya Krishna Menon, Sanjiv Kumar, and Vaishnavh  
557 Nagarajan. Think before you speak: Training language models with pause tokens. *arXiv preprint*  
558 *arXiv:2310.02226*, 2023.

559 Tianyu Guo, Druv Pai, Yu Bai, Jiantao Jiao, Michael I Jordan, and Song Mei. Active-dormant  
560 attention heads: Mechanistically demystifying extreme-token phenomena in llms. *arXiv preprint*  
561 *arXiv:2410.13835*, 2024.

563 Tianyu Guo, Hanlin Zhu, Ruiqi Zhang, Jiantao Jiao, Song Mei, Michael I Jordan, and Stuart Russell.  
564 How do llms perform two-hop reasoning in context? *arXiv preprint arXiv:2502.13913*, 2025.

565 Shibo Hao, Sainbayar Sukhbaatar, DiJia Su, Xian Li, Zhiting Hu, Jason Weston, and Yuandong  
566 Tian. Training large language models to reason in a continuous latent space. *arXiv preprint*  
567 *arXiv:2412.06769*, 2024.

569 Yixiao Huang, Hanlin Zhu, Tianyu Guo, Jiantao Jiao, Somayeh Sojoudi, Michael I Jordan, Stuart  
570 Russell, and Song Mei. Generalization or hallucination? understanding out-of-context reasoning  
571 in transformers. *arXiv preprint arXiv:2506.10887*, 2025.

573 Yu Huang, Yuan Cheng, and Yingbin Liang. In-context convergence of transformers. In *Proceedings*  
574 *of the 41st International Conference on Machine Learning*, pp. 19660–19722, 2024.

575 Samy Jelassi, Michael Sander, and Yuanzhi Li. Vision transformers provably learn spatial structure.  
576 *Advances in Neural Information Processing Systems*, 35:37822–37836, 2022.

578 Tushar Khot, Harsh Trivedi, Matthew Finlayson, Yao Fu, Kyle Richardson, Peter Clark, and Ashish  
579 Sabharwal. Decomposed prompting: A modular approach for solving complex tasks. *arXiv*  
580 *preprint arXiv:2210.02406*, 2022.

581 Juno Kim and Taiji Suzuki. Transformers provably solve parity efficiently with chain of thought.  
582 *arXiv preprint arXiv:2410.08633*, 2024.

584 Yingcong Li, Yixiao Huang, Muhammed E Ildiz, Ankit Singh Rawat, and Samet Oymak. Mechanics  
585 of next token prediction with self-attention. In *International Conference on Artificial Intelligence*  
586 *and Statistics*, pp. 685–693. PMLR, 2024a.

587 Zhiyuan Li, Hong Liu, Denny Zhou, and Tengyu Ma. Chain of thought empowers transformers to  
588 solve inherently serial problems. *arXiv preprint arXiv:2402.12875*, 1, 2024b.

590 Bingbin Liu, Jordan T Ash, Surbhi Goel, Akshay Krishnamurthy, and Cyril Zhang. Transformers  
591 learn shortcuts to automata. *arXiv preprint arXiv:2210.10749*, 2022.

593 Charles London and Varun Kanade. Pause tokens strictly increase the expressivity of constant-depth  
594 transformers. *arXiv preprint arXiv:2505.21024*, 2025.

594 Arvind Mahankali, Tatsunori B Hashimoto, and Tengyu Ma. One step of gradient descent is  
 595 provably the optimal in-context learner with one layer of linear self-attention. *arXiv preprint*  
 596 *arXiv:2307.03576*, 2023.

597 William Merrill and Ashish Sabharwal. The expressive power of transformers with chain of thought.  
 598 *arXiv preprint arXiv:2310.07923*, 2023.

600 Quan Nguyen and Thanh Nguyen-Tang. One-layer transformers are provably optimal for in-context  
 601 reasoning and distributional association learning in next-token prediction tasks. *arXiv preprint*  
 602 *arXiv:2505.15009*, 2025.

603 Eshaan Nichani, Alex Damian, and Jason D Lee. How transformers learn causal structure with  
 604 gradient descent. *arXiv preprint arXiv:2402.14735*, 2024a.

606 Eshaan Nichani, Jason D Lee, and Alberto Bietti. Understanding factual recall in transformers via  
 607 associative memories. *arXiv preprint arXiv:2412.06538*, 2024b.

609 Jacob Pfau, William Merrill, and Samuel R Bowman. Let’s think dot by dot: Hidden computation  
 610 in transformer language models. *arXiv preprint arXiv:2404.15758*, 2024.

611 Zhihong Shao, Peiyi Wang, Qihao Zhu, Runxin Xu, Junxiao Song, Xiao Bi, Haowei Zhang,  
 612 Mingchuan Zhang, YK Li, Y Wu, et al. Deepseekmath: Pushing the limits of mathematical  
 613 reasoning in open language models. *arXiv preprint arXiv:2402.03300*, 2024.

615 Daniel Soudry, Elad Hoffer, Mor Shpigel Nacson, Suriya Gunasekar, and Nathan Srebro. The im-  
 616 plicit bias of gradient descent on separable data. *Journal of Machine Learning Research*, 19(70):  
 617 1–57, 2018.

618 DiJia Su, Hanlin Zhu, Yingchen Xu, Jiantao Jiao, Yuandong Tian, and Qingqing Zheng. Token  
 619 assorted: Mixing latent and text tokens for improved language model reasoning. *arXiv preprint*  
 620 *arXiv:2502.03275*, 2025.

622 Yuandong Tian, Yiping Wang, Beidi Chen, and Simon S Du. Scan and snap: Understanding training  
 623 dynamics and token composition in 1-layer transformer. *Advances in neural information process-  
 624 ing systems*, 36:71911–71947, 2023a.

625 Yuandong Tian, Yiping Wang, Zhenyu Zhang, Beidi Chen, and Simon Du. Joma: Demystifying mul-  
 626 tilayer transformers via joint dynamics of mlp and attention. *arXiv preprint arXiv:2310.00535*,  
 627 2023b.

628 Peiyi Wang, Lei Li, Zhihong Shao, RX Xu, Damai Dai, Yifei Li, Deli Chen, Yu Wu, and Zhifang  
 629 Sui. Math-shepherd: Verify and reinforce llms step-by-step without human annotations. *arXiv*  
 630 *preprint arXiv:2312.08935*, 2023a.

632 Xinyi Wang, Lucas Caccia, Oleksiy Ostapenko, Xingdi Yuan, William Yang Wang, and Alessan-  
 633 dro Sordoni. Guiding language model reasoning with planning tokens. *arXiv preprint*  
 634 *arXiv:2310.05707*, 2023b.

635 Jason Wei, Xuezhi Wang, Dale Schuurmans, Maarten Bosma, Fei Xia, Ed Chi, Quoc V Le, Denny  
 636 Zhou, et al. Chain-of-thought prompting elicits reasoning in large language models. *Advances in*  
 637 *neural information processing systems*, 35:24824–24837, 2022.

639 Kaiyue Wen, Huaqing Zhang, Hongzhou Lin, and Jingzhao Zhang. From sparse dependence to  
 640 sparse attention: unveiling how chain-of-thought enhances transformer sample efficiency. *arXiv*  
 641 *preprint arXiv:2410.05459*, 2024.

642 Longhui Yu, Weisen Jiang, Han Shi, Jincheng Yu, Zhengying Liu, Yu Zhang, James T Kwok, Zhen-  
 643 guo Li, Adrian Weller, and Weiyang Liu. Metamath: Bootstrap your own mathematical questions  
 644 for large language models. *arXiv preprint arXiv:2309.12284*, 2023.

646 Xiang Yue, Xingwei Qu, Ge Zhang, Yao Fu, Wenhao Huang, Huan Sun, Yu Su, and Wenhui Chen.  
 647 Mammoth: Building math generalist models through hybrid instruction tuning. *arXiv preprint*  
*arXiv:2309.05653*, 2023.

648 Ruiqi Zhang, Spencer Frei, and Peter L Bartlett. Trained transformers learn linear models in-context.  
649 *Journal of Machine Learning Research*, 25(49):1–55, 2024.  
650

651 Denny Zhou, Nathanael Schärli, Le Hou, Jason Wei, Nathan Scales, Xuezhi Wang, Dale Schuur-  
652 mans, Claire Cui, Olivier Bousquet, Quoc Le, et al. Least-to-most prompting enables complex  
653 reasoning in large language models. *arXiv preprint arXiv:2205.10625*, 2022.

654 Hanlin Zhu, Baihe Huang, Shaolun Zhang, Michael Jordan, Jiantao Jiao, Yuandong Tian, and Stu-  
655 art J Russell. Towards a theoretical understanding of the ‘reversal curse’ via training dynamics.  
656 *Advances in Neural Information Processing Systems*, 37:90473–90513, 2024.

657 Hanlin Zhu, Shibo Hao, Zhiting Hu, Jiantao Jiao, Stuart Russell, and Yuandong Tian. Reason-  
658 ing by superposition: A theoretical perspective on chain of continuous thought. *arXiv preprint  
arXiv:2505.12514*, 2025.

661  
662  
663  
664  
665  
666  
667  
668  
669  
670  
671  
672  
673  
674  
675  
676  
677  
678  
679  
680  
681  
682  
683  
684  
685  
686  
687  
688  
689  
690  
691  
692  
693  
694  
695  
696  
697  
698  
699  
700  
701

702 **A NOTATION DETAILS**  
703

704 The notation and meaning of each token and the position index are the same as Zhu et al. (2025).  
 705 For completeness, we provide detailed descriptions of different tokens in Table 1 (which is Table 2  
 706 in Zhu et al. (2025)), and the position index of different tokens or continuous thoughts in Table 2  
 707 (which is Table 3 in Zhu et al. (2025)).

Tokens	Meanings
$<\text{s}>$	a special token denoting the beginning of the sentence
$s_i$	the source node of edge $i$
$t_i$	the target node of edge $i$
$<\text{e}>$	a special token marking the end of an edge
$<\text{Q}>$	a special token followed by two candidate nodes
$c_1, c_2$	two candidate destination nodes
$<\text{R}>$	a special token marking the start of reasoning
$r$	the root node
$[t_i]$	the $i$ -th continuous thought (represented by a $d$ -dimensional vector)
$<\text{A}>$	a special token driving the model to make the final prediction

720  
721 Table 1: Meaning of each token (Table 2 in Zhu et al. (2025)).  
722

Notations	Position indices
$\text{Idx}(<\text{s}>)$	1
$\text{Idx}(s_i)$	$3i - 1$
$\text{Idx}(t_i)$	$3i$
$\text{Idx}(<\text{e}>, i)$	$3i + 1$
$\text{Idx}(<\text{Q}>)$	$3m + 2$
$\text{Idx}(c_1)$	$3m + 3$
$\text{Idx}(c_2)$	$3m + 4$
$\text{Idx}(<\text{R}>)$	$3m + 5$
$\text{Idx}(r)$	$3m + 6 = t_0$
$\text{Idx}([t_i])$	$t_0 + i$
$\text{Idx}(<\text{A}>)$	$t_0 + C + 1 = T$

736 Table 2: Position indices of different tokens or continuous thoughts in the input sequence (Table 3  
737 in Zhu et al. (2025)).  
738740 **B MISSING PROOFS FOR SECTION 3**  
741

742 In this section, we provide the full proof of theoretical results in Section 3. We first provide theoretical  
 743 analysis of COCONUT-BFS and COCONUT in Appendix B.1, Appendix B.2, respectively, and  
 744 provide results for continuous thought expansion in Appendix B.3.

745 **B.1 ANALYSIS OF COCONUT-BFS**  
746

747 In this section, we analyze the training dynamics of COCONUT-BFS. We first provide the closed-  
 748 form formulation of the gradient  $\nabla_{\mu_v} \ell_{\mathcal{G}, r}^{\text{BFS}} = \nabla_{\mu_v} \ell_{\mathcal{G}, r}^{\text{BFS}}(\mu)$ , where  $\mu = \{\mu_v\}_{v \in \mathcal{V}}$  is the set of  
 749 parameters. We omit the superscript or subscript when the context is clear.

750 **Lemma 3** (Per-instance gradient of  $\mu_v$  for COCONUT-BFS). *Under the loss function of COCONUT-  
 751 BFS as given in (5) and the forward pass as in (2), the per-instance gradient is*

$$753 \nabla_{\mu_v} \ell(\mu) = -\frac{\mathbb{1}\{v \in \mathcal{N}_c\}}{\sqrt{|\mathcal{N}_c|}} \cdot \frac{\sum_{v':(v \rightarrow v') \in \mathcal{E}} \exp(\xi_{v'})}{\exp(\xi_+)} \cdot \frac{n - |\mathcal{N}_{c+1}|}{\exp(\xi_+) + n - |\mathcal{N}_{c+1}|}$$

755 for any  $v \in \mathcal{V}$ , where  $\xi_+ = \log \left( \sum_{v \in \mathcal{N}_{c+1}} \exp(\xi_v) \right)$ .

756 *Proof.* First, note that for any  $v \in \mathcal{V}$ , according to (2), the logit can be calculated as

$$\begin{aligned}
 \xi_v &= \mathbb{E}(v)^\top (\mathbf{h}_{[\mathbf{t}_c]} + \phi(\mathbf{h}_{[\mathbf{t}_c]}; \{\mathbf{h}_i\}_{i=1}^m)) \\
 &= \mathbb{E}(v)^\top \left( \mathbf{h}_{[\mathbf{t}_c]} + \mathbf{V} \sum_{i=1}^m \sigma(\mathbf{h}_{[\mathbf{t}_c]}^\top \mathbf{W} \mathbf{h}_i) \mathbf{h}_i \right) \\
 &= \mathbb{E}(v)^\top \left( \mathbf{h}_{[\mathbf{t}_c]} + \sum_{i=1}^m (\mathbf{h}_{[\mathbf{t}_c]}^\top \mathbf{W} \mathbf{h}_i) \mathbf{h}_i \right) \\
 &= \mathbb{E}(v)^\top \left( \mathbf{h}_{[\mathbf{t}_c]} + \sum_{i=1}^m \left( \left( \sum_{v' \in \mathcal{N}_c} \lambda \mathbb{E}(v') \right)^\top \sum_{v' \in \mathcal{V}} \mu_{v'} \mathbb{E}(v') \mathbb{E}_s(v')^\top (\mathbb{E}_s(s_i) + \mathbb{E}_t(t_i)) \right) \mathbf{h}_i \right) \\
 &= \mathbb{E}(v)^\top \left( \mathbf{h}_{[\mathbf{t}_c]} + \sum_{i=1}^m \left( \left( \sum_{v' \in \mathcal{N}_c} \lambda \mathbb{E}(v') \right)^\top \mu_{s_i} \mathbb{E}(s_i) \right) \mathbf{h}_i \right) \\
 &= \mathbb{E}(v)^\top \left( \mathbf{h}_{[\mathbf{t}_c]} + \sum_{i=1}^m \lambda \mu_{s_i} \mathbb{1}\{s_i \in \mathcal{N}_c\} \mathbf{h}_i \right) \\
 &= \lambda \cdot \mathbb{1}\{v \in \mathcal{N}_c\} + \sum_{i=1}^m \lambda \mu_{s_i} \mathbb{1}\{s_i \in \mathcal{N}_c\} \cdot \mathbb{1}\{v = t_i\},
 \end{aligned}$$

777 where  $\lambda = \frac{1}{\sqrt{|\mathcal{N}_c|}}$ . Note that by the definition of  $\mathcal{N}_c$ , we have  $\xi_v = 0$  if  $v \notin \mathcal{N}_{c+1}$ . Therefore,

$$\begin{aligned}
 \ell(\boldsymbol{\mu}) &= -\log \frac{\sum_{v \in \mathcal{N}_{c+1}} \exp(\xi_v)}{\sum_{v \in \mathcal{V}} \exp(\xi_v)} \\
 &= -\log \frac{\sum_{v \in \mathcal{N}_{c+1}} \exp(\lambda \cdot \mathbb{1}\{v \in \mathcal{N}_c\} + \sum_{i=1}^m \lambda \mu_{s_i} \mathbb{1}\{s_i \in \mathcal{N}_c\} \cdot \mathbb{1}\{v = t_i\})}{\sum_{v \in \mathcal{V}} \exp(\lambda \cdot \mathbb{1}\{v \in \mathcal{N}_c\} + \sum_{i=1}^m \lambda \mu_{s_i} \mathbb{1}\{s_i \in \mathcal{N}_c\} \cdot \mathbb{1}\{v = t_i\})} \\
 &= -\log \left( 1 - \frac{n - |\mathcal{N}_{c+1}|}{\sum_{v \in \mathcal{V}} \exp(\lambda \cdot \mathbb{1}\{v \in \mathcal{N}_c\} + \sum_{i=1}^m \lambda \mu_{s_i} \mathbb{1}\{s_i \in \mathcal{N}_c\} \cdot \mathbb{1}\{v = t_i\})} \right).
 \end{aligned}$$

786 For simplicity, we define  $\exp(\xi_+) = \sum_{v \in \mathcal{N}_{c+1}} \exp(\xi_v)$  and thus

$$\ell(\boldsymbol{\mu}) = -\log \left( 1 - \frac{n - |\mathcal{N}_{c+1}|}{\exp(\xi_+) + n - |\mathcal{N}_{c+1}|} \right).$$

790 Then the per-instance gradient can be calculated as

$$\begin{aligned}
 \nabla_{\mu_v} \ell(\boldsymbol{\mu}) &= -\frac{\exp(\xi_+) + n - |\mathcal{N}_{c+1}|}{\exp(\xi_+)} \cdot \frac{n - |\mathcal{N}_{c+1}|}{(\exp(\xi_+) + n - |\mathcal{N}_{c+1}|)^2} \cdot \nabla_{\mu_v} \exp(\xi_+) \\
 &= -\frac{\sum_{v' \in \mathcal{N}_{c+1}} \exp(\xi_{v'}) \mathbb{1}\{v \in \mathcal{N}_c\} \sum_{i=1}^m \lambda \mathbb{1}\{s_i = v, t_i = v'\}}{\exp(\xi_+)} \cdot \frac{n - |\mathcal{N}_{c+1}|}{\exp(\xi_+) + n - |\mathcal{N}_{c+1}|} \\
 &= -\lambda \cdot \mathbb{1}\{v \in \mathcal{N}_c\} \frac{\sum_{v':(v \rightarrow v') \in \mathcal{E}} \exp(\xi_{v'})}{\exp(\xi_+)} \cdot \frac{n - |\mathcal{N}_{c+1}|}{\exp(\xi_+) + n - |\mathcal{N}_{c+1}|}.
 \end{aligned}$$

□

802 Now we calculate the gradient of  $\mu_v$  over the whole dataset, where the nodes of the graphs are  
803 randomly shuffled. We also write  $\mathcal{L}^{\text{BFS}} = \mathcal{L}^{\text{BFS}}(\boldsymbol{\mu})$  and omit the superscript when the context is  
804 clear.

805 **Lemma 4** (Whole-dataset gradient of  $\mu_v$  for COCONUT-BFS). *Under the loss function of*  
806 *COCONUT-BFS as given in (5) and the forward pass as in (2) and assuming all  $\mu_v$  have the same*  
807 *value, the gradient w.r.t. the whole dataset is*

$$\nabla_{\mu_v} \mathcal{L}(\boldsymbol{\mu}) = -\frac{\exp(-\xi_+)}{n \cdot \sqrt{|\mathcal{N}_c|}} \cdot \frac{n - |\mathcal{N}_{c+1}|}{\exp(\xi_+) + n - |\mathcal{N}_{c+1}|} \sum_{v \in \mathcal{V}} d_v \exp(\xi_v)$$

810 for any  $v \in \mathcal{V}$  which is independent of  $v$ , where  $\xi_+ = \log \left( \sum_{v \in \mathcal{N}_{c+1}} \exp(\xi_v) \right)$ .  
 811  
 812  
 813  
 814

815 *Proof.* Denote  $\xi_+^{(\mathcal{G}, r)} = \log \left( \sum_{v \in \mathcal{N}_{c+1}^{\mathcal{G}}(r)} \exp(\xi_v^{(\mathcal{G}, r)}) \right)$ , where  $\xi_v^{(\mathcal{G}, r)}$  is the logit of  $v$  when the  
 816 graph in the prompt is  $\mathcal{G}$  and the start node is  $r$ .  
 817

818 According to Lemma 3 and the condition that all  $\mu_v$  have the same value, for any permutation  
 819  $\pi \in S_{\mathcal{V}}$ , we have

$$\begin{aligned} 820 \quad & \xi_{\pi(v)}^{(\pi(\mathcal{G}), \pi(r))} \\ 821 \quad &= \frac{\mathbb{1}\{\pi(v) \in \mathcal{N}_c^{\pi(\mathcal{G})}(\pi(r))\} + \sum_{i=1}^m \mu_{\pi(s_i)} \mathbb{1}\{\pi(s_i) \in \mathcal{N}_c^{\pi(\mathcal{G})}(\pi(r))\} \cdot \mathbb{1}\{\pi(v) = \pi(t_i)\}}{\sqrt{|\mathcal{N}_c^{\pi(\mathcal{G})}(\pi(r))|}} \\ 822 \quad &= \frac{1}{\sqrt{|\mathcal{N}_c^{\mathcal{G}}(r)|}} \left( \mathbb{1}\{v \in \mathcal{N}_c^{\mathcal{G}}(r)\} + \sum_{i=1}^m \mu_{s_i} \mathbb{1}\{s_i \in \mathcal{N}_c^{\mathcal{G}}(r)\} \cdot \mathbb{1}\{v = t_i\} \right) \\ 823 \quad &= \xi_v^{(\mathcal{G}, r)}. \end{aligned}$$

831 This also implies  
 832

$$\begin{aligned} 833 \quad & \exp(\xi_+^{(\pi(\mathcal{G}), \pi(r))}) = \sum_{\pi(v) \in \mathcal{N}_{c+1}^{\pi(\mathcal{G})}(\pi(r))} \exp(\xi_{\pi(v)}^{(\pi(\mathcal{G}), \pi(r))}) \\ 834 \quad &= \sum_{v \in \mathcal{N}_{c+1}^{\mathcal{G}}(r)} \exp(\xi_v^{(\mathcal{G}, r)}) \\ 835 \quad &= \exp(\xi_+^{(\mathcal{G}, r)}). \end{aligned}$$

841 Therefore, by Lemma 3, we can obtain that  
 842

$$\begin{aligned} 843 \quad & \nabla_{\mu_{\pi(v)}} \ell_{\pi(\mathcal{G}), \pi(r)}(\boldsymbol{\mu}) \\ 844 \quad &= -\frac{\mathbb{1}\{\pi(v) \in \mathcal{N}_c^{\pi(\mathcal{G})}(\pi(r))\}}{\sqrt{|\mathcal{N}_c^{\pi(\mathcal{G})}(\pi(r))|}} \cdot \frac{\sum_{\pi(v'): (\pi(v) \rightarrow \pi(v')) \in \pi(\mathcal{E})} \exp(\xi_{\pi(v')}^{(\pi(\mathcal{G}), \pi(r))})}{\exp(\xi_+^{(\pi(\mathcal{G}), \pi(r))})} \\ 845 \quad & \quad \cdot \frac{n - |\mathcal{N}_{c+1}^{\pi(\mathcal{G})}(\pi(r))|}{\exp(\xi_+^{(\pi(\mathcal{G}), \pi(r))}) + n - |\mathcal{N}_{c+1}^{\pi(\mathcal{G})}(\pi(r))|} \\ 846 \quad &= -\frac{\mathbb{1}\{v \in \mathcal{N}_c^{\mathcal{G}}(r)\}}{\sqrt{|\mathcal{N}_c^{\mathcal{G}}(r)|}} \cdot \frac{\sum_{v': (v \rightarrow v') \in \mathcal{E}} \exp(\xi_{v'}^{(\mathcal{G}, r)})}{\exp(\xi_+^{(\mathcal{G}, r)})} \cdot \frac{n - |\mathcal{N}_{c+1}^{\mathcal{G}}(r)|}{\exp(\xi_+^{(\mathcal{G}, r)}) + n - |\mathcal{N}_{c+1}^{\mathcal{G}}(r)|} \\ 847 \quad &= \nabla_{\mu_v} \ell_{\mathcal{G}, r}(\boldsymbol{\mu}). \end{aligned}$$

858 Therefore, we can calculate the gradient with respect to the whole dataset as  
 859

$$\begin{aligned} 860 \quad & \nabla_{\mu_v} \mathcal{L}(\boldsymbol{\mu}) = \mathbb{E}_{\pi \sim \text{Unif}(S_{\mathcal{V}})} [\nabla_{\mu_v} \ell_{\pi(\mathcal{G}), \pi(r)}(\boldsymbol{\mu})] \\ 861 \quad &= \mathbb{E}_{\pi \sim \text{Unif}(S_{\mathcal{V}})} [\nabla_{\mu_{\pi^{-1}(v)}} \ell_{\mathcal{G}, r}(\boldsymbol{\mu})] \\ 862 \quad &= \mathbb{E}_{v' \sim \text{Unif}(\mathcal{V})} [\nabla_{\mu_{v'}} \ell_{\mathcal{G}, r}(\boldsymbol{\mu})] \end{aligned}$$

864 which is independent of  $v$  and thus the gradients for  $\mu_v$  are equal for all  $v \in \mathcal{V}$ . Furthermore, we  
 865 can calculate that

$$\begin{aligned}
 866 \quad & \nabla_{\mu_v} \mathcal{L}(\boldsymbol{\mu}) \\
 867 \quad &= \frac{1}{n} \sum_{v \in \mathcal{V}} \left( -\frac{\mathbb{1}\{v \in \mathcal{N}_c\}}{\sqrt{|\mathcal{N}_c|}} \cdot \frac{\sum_{v':(v \rightarrow v') \in \mathcal{E}} \exp(\xi_{v'})}{\exp(\xi_+)} \cdot \frac{n - |\mathcal{N}_{c+1}|}{\exp(\xi_+) + n - |\mathcal{N}_{c+1}|} \right) \\
 868 \quad &= -\frac{1}{n \cdot \sqrt{|\mathcal{N}_c|}} \cdot \frac{n - |\mathcal{N}_{c+1}|}{\exp(\xi_+) + n - |\mathcal{N}_{c+1}|} \sum_{v \in \mathcal{N}_c} \frac{\sum_{v':(v \rightarrow v') \in \mathcal{E}} \exp(\xi_{v'})}{\exp(\xi_+)} \\
 869 \quad &= -\frac{\exp(-\xi_+)}{n \cdot \sqrt{|\mathcal{N}_c|}} \cdot \frac{n - |\mathcal{N}_{c+1}|}{\exp(\xi_+) + n - |\mathcal{N}_{c+1}|} \sum_{v \in \mathcal{N}_c} \sum_{v':(v \rightarrow v') \in \mathcal{E}} \exp(\xi_{v'}) \\
 870 \quad &= -\frac{\exp(-\xi_+)}{n \cdot \sqrt{|\mathcal{N}_c|}} \cdot \frac{n - |\mathcal{N}_{c+1}|}{\exp(\xi_+) + n - |\mathcal{N}_{c+1}|} \sum_{v \in \mathcal{V}} d_v \exp(\xi_v).
 \end{aligned}$$

□

880 According to the gradient of  $\mu_v$ , we finally show that  $\mu_v$  diverges to infinity at least logarithmically  
 881 in  $t$ .

882 **Lemma 5** (Dynamics of  $\mu_v$  for COCONUT-BFS). *Let  $\mu_v(t)$  be the value of  $\mu_v$  at time  $t$ . Assume  
 883 zero-initialization, i.e.,  $\mu_v(0) = 0$  for all  $v \in \mathcal{V}$ . Under gradient flow*

$$884 \quad \dot{\mu}_v = -\alpha \cdot \nabla_{\mu_v} \mathcal{L}^{\text{BFS}}(\boldsymbol{\mu}) \quad (10)$$

885 where  $\alpha > 0$  is the learning rate, we have

$$886 \quad \mu_v(t) \geq c_1 \ln(1 + \alpha c_2 t)$$

887 for all  $v \in \mathcal{V}$  where  $c_1 = \frac{1}{2\sqrt{|\mathcal{N}_c|}}$ ,  $c_2 = n^{-3}e^{-2}$ .

888 *Proof.* First, by Lemma 4, all  $\dot{\mu}_v$  have the same value if all  $\mu_v$  have the same value. Given that  
 889  $\mu_v(0) = 0$  for all  $v \in \mathcal{V}$ , we can obtain that for any time  $t$ ,  $\mu_v(t)$  have the same value for all  $v \in \mathcal{V}$   
 890 using similar argument as in Lemma 15 of Huang et al. (2025).

891 Now, given any fixed time  $t \geq 0$ , it holds that  $\mu_v(t)$  has the same value for all  $v \in \mathcal{V}$ . We omit  $t$  for  
 892 notation convenience, i.e., using  $\mu_v$  to represent  $\mu_v(t)$ . Below, we first provide a lower bound of the  
 893 gradient  $\dot{\mu}_v$ .

894 Since we are guaranteed that one of  $c_1$  and  $c_2$  cannot be reached from  $r$ ,  $\mathcal{N}_{c+1}$  cannot contain all  
 895 the vertices in  $\mathcal{V}$  for any  $c$ , and thus  $n - |\mathcal{N}_{c+1}| \geq 1$ . Also, since one of  $c_1$  and  $c_2$  is guaranteed to  
 896 be reachable from  $r$ , there exists  $v \in \mathcal{V}$  such that  $d_v \geq 1$  for any  $c$ . This is because the start node  
 897  $r \in \mathcal{N}_0 \subseteq \mathcal{N}_c$  for any  $c \geq 0$ , and we can take  $v = p_1$  which is on the shortest path from  $r$  to  $c^*$ .  
 898 Therefore, we can obtain that  $\dot{\mu}_v > 0$ . Moreover, we have

$$\begin{aligned}
 900 \quad \dot{\mu}_v &= \alpha \cdot \frac{\exp(-\xi_+)}{n \cdot \sqrt{|\mathcal{N}_c|}} \cdot \frac{n - |\mathcal{N}_{c+1}|}{\exp(\xi_+) + n - |\mathcal{N}_{c+1}|} \sum_{v \in \mathcal{V}} d_v \exp(\xi_v) \\
 901 \quad &\geq \alpha \cdot \frac{\exp(-\xi_+)}{n \cdot \sqrt{|\mathcal{N}_c|}} \cdot \frac{1}{\exp(\xi_+) + 1} \sum_{v \in \mathcal{V}} d_v \exp(\xi_v) \\
 902 \quad &\geq \frac{\alpha}{n \cdot \sqrt{|\mathcal{N}_c|}} \cdot \frac{\sum_{v \in \mathcal{V}} d_v \exp(\xi_v)}{(\exp(\xi_+) + 1) \cdot \exp(\xi_r)}.
 \end{aligned}$$

903 Note that by definition, for any vertex  $v \in \mathcal{N}_{c+1} \setminus \{r\}$ , there must exists another vertex  $v' \in \mathcal{N}_c$   
 904 such that  $(v' \rightarrow v) \in \mathcal{E}$ , which implies that  $d_v \geq 1$ . Therefore,

$$\begin{aligned}
 905 \quad \sum_{v \in \mathcal{V}} d_v \exp(\xi_v) &\geq \sum_{v \in \mathcal{N}_{c+1} \setminus \{r\}} d_v \exp(\xi_v) \\
 906 \quad &\geq \sum_{v \in \mathcal{N}_{c+1} \setminus \{r\}} \exp(\xi_v) \\
 907 \quad &= \exp(\xi_+) - \exp(\xi_r),
 \end{aligned}$$

which further implies that

$$\begin{aligned}\dot{\mu}_v &\geq \frac{\alpha}{n \cdot \sqrt{|\mathcal{N}_c|}} \cdot \frac{\sum_{v \in \mathcal{V}} d_v \exp(\xi_v)}{(\exp(\xi_+) + 1) \cdot \exp(\xi_+)} \\ &\geq \frac{\alpha}{n \cdot \sqrt{|\mathcal{N}_c|}} \cdot \frac{\exp(\xi_+) - \exp(\xi_r)}{(\exp(\xi_+) + 1) \cdot \exp(\xi_+)}.\end{aligned}$$

Now recall from Lemma 3 that

$$\begin{aligned}\xi_v &= \frac{1}{\sqrt{|\mathcal{N}_c|}} \left( \mathbb{1}\{v \in \mathcal{N}_c\} + \sum_{i=1}^m \mu_{s_i} \mathbb{1}\{s_i \in \mathcal{N}_c\} \cdot \mathbb{1}\{v = t_i\} \right) \\ &= \frac{1}{\sqrt{|\mathcal{N}_c|}} (\mathbb{1}\{v \in \mathcal{N}_c\} + d_v \cdot \mu_v) \\ &\leq \frac{1}{\sqrt{|\mathcal{N}_c|}} (1 + |\mathcal{N}_c| \cdot \mu_v).\end{aligned}$$

Therefore,

$$\begin{aligned}\exp(\xi_+) &= \sum_{v \in \mathcal{N}_{c+1}} \exp(\xi_v) \\ &\leq |\mathcal{N}_{c+1}| \exp \left( \frac{1}{\sqrt{|\mathcal{N}_c|}} (1 + |\mathcal{N}_c| \cdot \mu_v) \right) \\ &\leq n \cdot \exp \left( 1 + \sqrt{|\mathcal{N}_c|} \cdot \mu_v \right).\end{aligned}$$

Also, since  $p_1 \in \mathcal{N}_{c+1}$  and  $\deg_{\mathcal{G}, \mathcal{N}_c}^-(p_1) \geq 1$ , we can obtain that

$$\begin{aligned}\exp(\xi_+) - \exp(\xi_r) &\geq \exp \left( \xi_{p_1}^{(\mathcal{G}, r)} \right) \\ &= \exp \left( \frac{1}{\sqrt{|\mathcal{N}_c|}} (\mathbb{1}\{p_1 \in \mathcal{N}_c\} + d_{p_1} \cdot \mu_v) \right) \\ &\geq \exp \left( \frac{\mu_v}{\sqrt{|\mathcal{N}_c|}} \right).\end{aligned}$$

Combining the above two inequalities, we can obtain that

$$\begin{aligned}\dot{\mu}_v &\geq \frac{\alpha}{n \cdot \sqrt{|\mathcal{N}_c|}} \cdot \frac{\exp(\xi_+) - \exp(\xi_r)}{(\exp(\xi_+) + 1) \cdot \exp(\xi_+)} \\ &\geq \frac{\alpha}{n \cdot \sqrt{|\mathcal{N}_c|}} \cdot \frac{\exp \left( \frac{\mu_v}{\sqrt{|\mathcal{N}_c|}} \right)}{2n^2 \cdot \exp \left( 2 + 2\sqrt{|\mathcal{N}_c|} \cdot \mu_v \right)} \\ &\geq \frac{\alpha}{2n^3 e^2 \cdot \sqrt{|\mathcal{N}_c|}} \cdot \exp \left( -2\sqrt{|\mathcal{N}_c|} \cdot \mu_v \right).\end{aligned}$$

Finally, by applying Lemma 13, we can obtain that

$$\mu_v(t) \geq \frac{1}{2\sqrt{|\mathcal{N}_c|}} \ln \left( 1 + \alpha n^{-3} e^{-2} t \right).$$

□

## B.2 ANALYSIS OF COCONUT

In this section, we analyze the training dynamics of COCONUT. Similarly, we first provide the closed-form formulation of the gradient  $\nabla_{\mu_v} \ell_{\mathcal{G}, r, p}^{\text{coco}} = \nabla_{\mu_v} \ell_{\mathcal{G}, r, p}^{\text{coco}}(\boldsymbol{\mu})$ , where  $\boldsymbol{\mu} = \{\mu_v\}_{v \in \mathcal{V}}$  is the set of parameters. We omit the superscript or subscript when the context is clear.

972     **Lemma 6** (Per-instance gradient of  $\mu_v$  for COCONUT). *Under the loss function of COCONUT as  
973     given in (6) and the forward pass as in (2), the per-instance gradient is*  
974

$$975 \quad \nabla_{\mu_v} \ell(\boldsymbol{\mu}) = \frac{\mathbb{1}\{v \in \mathcal{N}_c\}}{\sqrt{|\mathcal{N}_c|}} \left( -\mathbb{1}\{(v \rightarrow p_{c+1}) \in \mathcal{E}\} + \frac{\sum_{v':(v \rightarrow v') \in \mathcal{E}} \exp(\xi_{v'})}{\exp(\xi_+) + n - |\mathcal{N}_{c+1}|} \right)$$

978     for any  $v \in \mathcal{V}$ , where  $\xi_+ = \log \left( \sum_{v \in \mathcal{N}_{c+1}} \exp(\xi_v) \right)$ .  
979

980     *Proof.* First, according to the proof of Lemma 3, we have  
981

$$982 \quad \xi_v = \lambda \cdot \mathbb{1}\{v \in \mathcal{N}_c\} + \sum_{i=1}^m \lambda \mu_{s_i} \mathbb{1}\{s_i \in \mathcal{N}_c\} \cdot \mathbb{1}\{v = t_i\},$$

985     where  $\lambda = \frac{1}{\sqrt{|\mathcal{N}_c|}}$ . Note that by the definition of  $\mathcal{N}_c$ , we have  $\xi_v = 0$  if  $v \notin \mathcal{N}_{c+1}$ . Therefore,  
986

$$988 \quad \ell(\boldsymbol{\mu}) = -\log \frac{\exp(\xi_{p_{c+1}})}{\sum_{v \in \mathcal{V}} \exp(\xi_v)} = -\log \left( \frac{\exp(\xi_{p_{c+1}})}{\exp(\xi_+) + n - |\mathcal{N}_{c+1}|} \right),$$

991     where  $\exp(\xi_+) = \sum_{v \in \mathcal{N}_{c+1}} \exp(\xi_v)$ .  
992

993     Then the per-instance gradient can be calculated as  
994

$$\begin{aligned} & \nabla_{\mu_v} \ell(\boldsymbol{\mu}) \\ &= -\frac{\exp(\xi_+) + n - |\mathcal{N}_{c+1}|}{\exp(\xi_{p_{c+1}})} \\ & \quad \cdot \frac{\nabla_{\mu_v} \exp(\xi_{p_{c+1}}) \cdot (\exp(\xi_+) + n - |\mathcal{N}_{c+1}|) - \exp(\xi_{p_{c+1}}) \nabla_{\mu_v} \exp(\xi_+)}{(\exp(\xi_+) + n - |\mathcal{N}_{c+1}|)^2} \\ &= -\frac{\nabla_{\mu_v} \exp(\xi_{p_{c+1}})}{\exp(\xi_{p_{c+1}})} + \frac{\nabla_{\mu_v} \exp(\xi_+)}{\exp(\xi_+) + n - |\mathcal{N}_{c+1}|} \\ &= -\nabla_{\mu_v} \xi_{p_{c+1}} + \frac{\nabla_{\mu_v} \exp(\xi_+)}{\exp(\xi_+) + n - |\mathcal{N}_{c+1}|}. \end{aligned}$$

1003     Since  
1004

$$\begin{aligned} \nabla_{\mu_v} \exp(\xi_+) &= \sum_{v' \in \mathcal{N}_{c+1}} \exp(\xi_{v'}) \mathbb{1}\{v \in \mathcal{N}_c\} \sum_{i=1}^m \lambda \mathbb{1}\{s_i = v, t_i = v'\} \\ &= \lambda \cdot \mathbb{1}\{v \in \mathcal{N}_c\} \sum_{v':(v \rightarrow v') \in \mathcal{E}} \exp(\xi_{v'}) \end{aligned}$$

1013     and  
1014

$$1015 \quad \nabla_{\mu_v} \xi_{p_{c+1}} = \lambda \cdot \mathbb{1}\{v \in \mathcal{N}_c\} \cdot \mathbb{1}\{(v \rightarrow p_{c+1}) \in \mathcal{E}\},$$

1017     we can finally obtain that  
1018

$$1019 \quad \nabla_{\mu_v} \ell(\boldsymbol{\mu}) = \frac{\mathbb{1}\{v \in \mathcal{N}_c\}}{\sqrt{|\mathcal{N}_c|}} \left( -\mathbb{1}\{(v \rightarrow p_{c+1}) \in \mathcal{E}\} + \frac{\sum_{v':(v \rightarrow v') \in \mathcal{E}} \exp(\xi_{v'})}{\exp(\xi_+) + n - |\mathcal{N}_{c+1}|} \right).$$

1022     □  
1023

1024     Now we calculate the gradient of  $\mu_v$  over the whole dataset, where the nodes of the graphs are  
1025     randomly shuffled. We also write  $\mathcal{L}^{\text{coco}} = \mathcal{L}^{\text{coco}}(\boldsymbol{\mu})$  and omit the superscript when the context is  
clear.

1026 **Lemma 7** (Whole-dataset gradient of  $\mu_v$  for COCONUT). *Under the loss function of COCONUT as*  
 1027 *given in (6) and the forward pass as in (2) and assuming all  $\mu_v$  have the same value, the gradient*  
 1028 *w.r.t. the whole dataset is*

$$1029 \quad \nabla_{\mu_v} \mathcal{L}(\boldsymbol{\mu}) = \frac{1}{n \cdot \sqrt{|\mathcal{N}_c|}} \left( -d_{p_{c+1}} + \frac{\sum_{v \in \mathcal{N}_{c+1}} d_v \exp(\xi_v)}{\exp(\xi_+) + n - |\mathcal{N}_{c+1}|} \right)$$

1030 *for any  $v \in \mathcal{V}$  which is independent of  $v$ , where  $\xi_+ = \log \left( \sum_{v \in \mathcal{N}_{c+1}} \exp(\xi_v) \right)$ .*

1031 *Proof.* Similar to Lemma 4, we denote  $\xi_+^{(\mathcal{G}, \mathbf{r})} = \log \left( \sum_{v \in \mathcal{N}_{c+1}^{(\mathcal{G}, \mathbf{r})}} \exp \left( \xi_v^{(\mathcal{G}, \mathbf{r})} \right) \right)$ , where  $\xi_v^{(\mathcal{G}, \mathbf{r})}$  is  
 1032 the logit of  $v$  when the graph in the prompt is  $\mathcal{G}$  and the start node is  $\mathbf{r}$ . According to the proof of  
 1033 Lemma 4, for any permutation  $\pi \in S_{\mathcal{V}}$ , we have

$$1034 \quad \xi_{\pi(v)}^{(\pi(\mathcal{G}), \pi(\mathbf{r}))} = \xi_v^{(\mathcal{G}, \mathbf{r})}$$

1035 for any  $v \in \mathcal{V}$  and

$$1036 \quad \exp \left( \xi_+^{(\pi(\mathcal{G}), \pi(\mathbf{r}))} \right) = \exp \left( \xi_+^{(\mathcal{G}, \mathbf{r})} \right).$$

1037 Therefore, by Lemma 6, we can obtain that

$$1038 \quad \begin{aligned} & \nabla_{\mu_{\pi(v)}} \ell_{\pi(\mathcal{G}), \pi(\mathbf{r}), \pi(p)}(\boldsymbol{\mu}) \\ &= \frac{\mathbb{1}\{\pi(v) \in \mathcal{N}_c^{\pi(\mathcal{G})}(\pi(\mathbf{r}))\}}{\sqrt{|\mathcal{N}_c^{\pi(\mathcal{G})}(\pi(\mathbf{r}))|}} (-\mathbb{1}\{(\pi(v) \rightarrow \pi(p_{c+1})) \in \pi(\mathcal{E})\} \\ & \quad + \frac{\sum_{\pi(v'): (\pi(v) \rightarrow \pi(v')) \in \pi(\mathcal{E})} \exp \left( \xi_{\pi(v')}^{(\pi(\mathcal{G}), \pi(\mathbf{r}))} \right)}{\exp \left( \xi_+^{(\mathcal{G}, \mathbf{r})} \right) + n - |\mathcal{N}_{c+1}^{\pi(\mathcal{G})}(\pi(\mathbf{r}))|}) \\ &= \frac{\mathbb{1}\{v \in \mathcal{N}_c^{\mathcal{G}}(\mathbf{r})\}}{\sqrt{|\mathcal{N}_c^{\mathcal{G}}(\mathbf{r})|}} \left( -\mathbb{1}\{(v \rightarrow p_{c+1}) \in \mathcal{E}\} + \frac{\sum_{v': (v \rightarrow v') \in \mathcal{E}} \exp \left( \xi_{v'}^{(\mathcal{G}, \mathbf{r})} \right)}{\exp \left( \xi_+^{(\mathcal{G}, \mathbf{r})} \right) + n - |\mathcal{N}_{c+1}^{\mathcal{G}}(\mathbf{r})|} \right) \\ &= \nabla_{\mu_v} \ell_{\mathcal{G}, \mathbf{r}, p}(\boldsymbol{\mu}). \end{aligned}$$

1039 Therefore, we can calculate the gradient with respect to the whole dataset as

$$1040 \quad \begin{aligned} \nabla_{\mu_v} \mathcal{L}(\boldsymbol{\mu}) &= \mathbb{E}_{\pi \sim \text{Unif}(S_{\mathcal{V}})} [\nabla_{\mu_v} \ell_{\pi(\mathcal{G}), \pi(\mathbf{r}), \pi(p)}(\boldsymbol{\mu})] \\ &= \mathbb{E}_{\pi \sim \text{Unif}(S_{\mathcal{V}})} [\nabla_{\mu_{\pi-1(v)}} \ell_{\mathcal{G}, \mathbf{r}, p, c}(\boldsymbol{\mu})] \\ &= \mathbb{E}_{v' \sim \text{Unif}(\mathcal{V})} [\nabla_{\mu_{v'}} \ell_{\mathcal{G}, \mathbf{r}, p, c}(\boldsymbol{\mu})] \end{aligned}$$

1041 which is independent of  $v$  and thus the gradients for  $\mu_v$  are equal for all  $v \in \mathcal{V}$ . Furthermore, similar  
 1042 to Lemma 4, we can calculate that

$$1043 \quad \begin{aligned} & \nabla_{\mu_v} \mathcal{L}(\boldsymbol{\mu}) \\ &= \frac{1}{n} \sum_{v \in \mathcal{V}} \frac{\mathbb{1}\{v \in \mathcal{N}_c\}}{\sqrt{|\mathcal{N}_c|}} \left( -\mathbb{1}\{(v \rightarrow p_{c+1}) \in \mathcal{E}\} + \frac{\sum_{v': (v \rightarrow v') \in \mathcal{E}} \exp(\xi_{v'})}{\exp(\xi_+) + n - |\mathcal{N}_{c+1}|} \right) \\ &= \frac{1}{n \cdot \sqrt{|\mathcal{N}_c|}} \left( -d_{p_{c+1}} + \frac{\sum_{v \in \mathcal{N}_{c+1}} d_v \exp(\xi_v)}{\exp(\xi_+) + n - |\mathcal{N}_{c+1}|} \right). \end{aligned}$$

1044  $\square$

1045 Finally, we derive the dynamics of  $\mu_v$ . Recall that we denote  $K = |\mathcal{N}_c|$ ,  $\lambda = \frac{1}{\sqrt{K}}$ . We also make  
 1046 the following notation for Theorem 4. Let  $d_{\star} := d_{p_{c+1}}$  and  $d_{\max} := \max_{u \in \mathcal{V}} d_u$ . Moreover, Let

1080  $c_0 := n - |\mathcal{N}_{c+1}| \geq 1$  and denote  
 1081

$$1082 \quad \xi_u(\mu) := \lambda (\mathbb{1}\{u \in \mathcal{N}_c\} + \mu d_u), \quad E_+(\mu) := \sum_{u \in \mathcal{N}_{c+1}} e^{\xi_u(\mu)},$$

$$1085 \quad S(\mu) := \sum_{u \in \mathcal{N}_{c+1}} d_u e^{\xi_u(\mu)}, \quad F(\mu) := \frac{S(\mu)}{E_+(\mu) + c_0}.$$

1087 **Theorem 4** (Dynamics of  $\mu_v$  for COCONUT). *Let  $\mu_v(t)$  be the value of  $\mu_v$  at time  $t$ . Assume zero-  
 1088 initialization, i.e.,  $\mu_v(0) = 0$  for all  $v \in \mathcal{V}$ . Under gradient flow  
 1089*

$$1090 \quad \dot{\mu}_v = -\alpha \cdot \nabla_{\mu_v} \mathcal{L}^{\text{coco}}(\boldsymbol{\mu}) \quad (11)$$

1091 where  $\alpha > 0$  is the learning rate, suppose the initialization satisfies  $\mu_v(0) = 0$  for all  $v$ . Then:

1093 1. **Scalar reduction.** For all  $t \geq 0$ ,  $\mu_v(t) \equiv \mu(t)$  is shared across  $v$ , and  $\mu(t)$  satisfies  
 1094

$$1095 \quad \boxed{\dot{\mu}(t) = \frac{\alpha}{n\sqrt{K}} (d_\star - F(\mu(t)))}. \quad (12)$$

1098 2. **Regularity of  $F$ .** The function  $F : \mathbb{R} \rightarrow \mathbb{R}$  is  $C^\infty$ , strictly increasing, and satisfies  
 1099

$$1100 \quad \lim_{\mu \rightarrow -\infty} F(\mu) = 0, \quad \lim_{\mu \rightarrow +\infty} F(\mu) = d_{\max}, \quad 0 < F(\mu) < d_{\max} \quad \text{for all finite } \mu.$$

1102 3. **Finite fixed point when  $d_\star < d_{\max}$ .** If  $d_\star < d_{\max}$ , there exists a unique  $\mu^* \in \mathbb{R}$  such that  
 1103  $F(\mu^*) = d_\star$ . The solution  $\mu(t)$  of (12) with  $\mu(0) = 0$  converges monotonically to  $\mu^*$ :

$$1105 \quad \mu(t) \nearrow \mu^* \quad \text{if } F(0) \leq d_\star, \quad \mu(t) \searrow \mu^* \quad \text{if } F(0) > d_\star,$$

1106 and the equilibrium  $\mu^*$  is locally exponentially stable, i.e., there exists  $\gamma > 0$  such that for  
 1107 all large enough  $t$ , it holds that  
 1108

$$1109 \quad |\mu(t) - \mu^*| \leq e^{-\gamma t} |\mu(0) - \mu^*|.$$

1111 4. **Logarithmic divergence when  $d_\star = d_{\max}$ .** If  $d_\star = d_{\max}$ , then  $\dot{\mu}(t) > 0$  for all  $t$  and  
 1112  $\mu(t) \rightarrow +\infty$ . Moreover, for all  $t \geq 0$ ,

$$1114 \quad \boxed{\mu(t) \geq \frac{1}{\lambda d_{\max}} \ln \left( 1 + \frac{\alpha \lambda d_{\max}^2 c_0 e^{-\lambda}}{2 n^2 \sqrt{K}} t \right)}. \quad (13)$$

1117 *Proof.* (1) **Scalar reduction.** By Lemma 7 and the similar argument as in the proof of Lemma 5, we  
 1118 have  $\mu_v(t) \equiv \mu(t)$  for all  $t \geq 0$ . Therefore, the gradient  $\nabla_{\mu_v} \mathcal{L}(\boldsymbol{\mu})$  is independent of  $v$  and equals  
 1119

$$1120 \quad \nabla_{\mu_v} \mathcal{L}(\boldsymbol{\mu}) = \frac{1}{n\sqrt{K}} \left( -d_\star + \frac{\sum_{u \in \mathcal{N}_{c+1}} d_u e^{\xi_u(\mu_u)}}{\sum_{u \in \mathcal{N}_{c+1}} e^{\xi_u(\mu_u)} + n - |\mathcal{N}_{c+1}|} \right) = \frac{1}{n\sqrt{K}} (-d_\star + F(\mu_v)).$$

1123 Thus, we have

$$1125 \quad \dot{\mu}(t) = -\nabla_{\mu_v} \mathcal{L}(\boldsymbol{\mu}(t)) = \frac{\alpha}{n\sqrt{K}} (d_\star - F(\mu(t))).$$

1127 (2) **Regularity and limits of  $F$ .** By the proof of Lemma 6 and the condition that  $\mu_v(t) \equiv \mu(t)$  for  
 1128 all  $v \in \mathcal{V}$  and  $t \geq 0$ , we have  
 1129

$$1130 \quad E_+(\mu) = \sum_{u \in \mathcal{N}_{c+1}} \exp(\lambda (\mathbb{1}\{u \in \mathcal{N}_c\} + \mu d_u)), \quad S(\mu) = \sum_{u \in \mathcal{N}_{c+1}} d_u \exp(\lambda (\mathbb{1}\{u \in \mathcal{N}_c\} + \mu d_u)).$$

1133 Both functions are finite sums of  $C^\infty$  functions of  $\mu$ , hence  $F(\mu) = S(\mu)/(E_+(\mu) + c_0)$  is also  
 $C^\infty$ .

Now we show the strict monotonicity of  $F(\cdot)$  on  $\mu$  by differentiation. We further write  $\xi_u := \xi_u(\mu)$  for brevity. Then

$$E'_+(\mu) = \lambda \sum_{u \in \mathcal{N}_{c+1}} d_u e^{\xi_u}, \quad S'(\mu) = \lambda \sum_{u \in \mathcal{N}_{c+1}} d_u^2 e^{\xi_u}.$$

Therefore, we can obtain that

$$\begin{aligned} F'(\mu) &= \frac{S'(\mu) (E_+(\mu) + c_0) - S(\mu) E'_+(\mu)}{(E_+(\mu) + c_0)^2} \\ &= \frac{\lambda}{(E_+(\mu) + c_0)^2} \left[ \left( \sum_{u \in \mathcal{N}_{c+1}} d_u^2 e^{\xi_u} \right) (E_+(\mu) + c_0) - \left( \sum_{u \in \mathcal{N}_{c+1}} d_u e^{\xi_u} \right)^2 \right]. \end{aligned}$$

Note that by the Cauchy-Schwarz inequality, we have

$$\sum_{u \in \mathcal{N}_{c+1}} d_u^2 e^{\xi_u} \cdot E_+(\mu) - \left( \sum_{u \in \mathcal{N}_{c+1}} d_u e^{\xi_u} \right)^2 \geq 0,$$

and hence

$$F'(\mu) \geq \frac{\lambda}{(E_+(\mu) + c_0)^2} c_0 E_+(\mu) \left( \sum_{u \in \mathcal{N}_{c+1}} d_u^2 e^{\xi_u} \right) > 0$$

since  $c_0 > 0$  and there exists at least one node  $u \in \mathcal{N}_{c+1}$  (e.g.,  $p_{c+1}$ ) such that  $d_u \geq 1$  by definition. Thus,  $F(\cdot)$  is strictly increasing.

Now we consider the limits of  $F(\cdot)$ . First, note that

$$S(\mu) = \sum_{u \in \mathcal{N}_{c+1}} d_u e^{\xi_u(\mu)},$$

and for each  $u \in \mathcal{N}_{c+1}$ , either  $d_u = 0$  or  $d_u > 0$  and thus

$$\lim_{\mu \rightarrow -\infty} d_u e^{\xi_u(\mu)} = \lim_{\mu \rightarrow -\infty} d_u \exp(\lambda(\mathbb{1}\{u \in \mathcal{N}_c\} + \mu d_u)) = 0.$$

Therefore, we have  $\lim_{\mu \rightarrow -\infty} S(\mu) = 0$ . Moreover, since  $E_+(\mu) + c_0 \geq c_0 > 0$ , we have

$$\lim_{\mu \rightarrow -\infty} F(\mu) = 0.$$

Now we consider the case when  $\mu \rightarrow +\infty$ . Since

$$\begin{aligned} \frac{e^{\xi_u(\mu)}}{E_+(\mu) + c_0} &= \frac{\exp(\lambda(\mathbb{1}\{u \in \mathcal{N}_c\} + \mu d_u))}{\sum_{v \in \mathcal{N}_{c+1}} \exp(\lambda(\mathbb{1}\{v \in \mathcal{N}_c\} + \mu d_v)) + c_0} \\ &= \frac{1}{\sum_{v \in \mathcal{N}_{c+1}} \exp(\lambda(\mathbb{1}\{v \in \mathcal{N}_c\} - \mathbb{1}\{u \in \mathcal{N}_c\} + \mu(d_v - d_u))) + c_0}. \end{aligned}$$

As  $\mu \rightarrow +\infty$ , we can obtain that if  $d_u < d_{\max}$ , then

$$\lim_{\mu \rightarrow +\infty} \frac{e^{\xi_u(\mu)}}{E_+(\mu) + c_0} \leq \lim_{\mu \rightarrow +\infty} \frac{1}{\exp(\lambda(-1 + \mu(d_{\max} - d_u))) + c_0} = 0.$$

If  $d_u = d_{\max}$ , then

$$\begin{aligned} \lim_{\mu \rightarrow +\infty} \frac{e^{\xi_u(\mu)}}{E_+(\mu) + c_0} &= \lim_{\mu \rightarrow +\infty} \frac{\exp(\lambda \cdot \mathbb{1}\{u \in \mathcal{N}_c\})}{\sum_{v \in D_{\max}} \exp(\lambda \cdot \mathbb{1}\{v \in \mathcal{N}_c\}) + \sum_{v \in \mathcal{N}_{c+1} \setminus D_{\max}} \exp(\lambda(\mathbb{1}\{v \in \mathcal{N}_c\} + \mu(d_v - d_{\max}))) + \frac{c_0}{e^{\lambda \mu d_{\max}}}} \\ &= \frac{\exp(\lambda \cdot \mathbb{1}\{u \in \mathcal{N}_c\})}{\sum_{v \in D_{\max}} \exp(\lambda \cdot \mathbb{1}\{v \in \mathcal{N}_c\})}, \end{aligned}$$

1188 where  $D_{\max} := \{u \in \mathcal{N}_{c+1} : d_u = d_{\max}\}$ . Therefore,

$$1190 \lim_{\mu \rightarrow +\infty} F(\mu) = \sum_{u \in D_{\max}} d_u \frac{\exp(\lambda \cdot \mathbb{1}\{u \in \mathcal{N}_c\})}{\sum_{v \in D_{\max}} \exp(\lambda \cdot \mathbb{1}\{v \in \mathcal{N}_c\})} = d_{\max}.$$

1193 Finally, the inequality  $F(\mu) < d_{\max}$  for finite  $\mu$  follows from  $S(\mu) \leq d_{\max} E_+(\mu)$  and  $c_0 > 0$ :

$$1195 F(\mu) = \frac{S(\mu)}{E_+(\mu) + c_0} \leq \frac{d_{\max} E_+(\mu)}{E_+(\mu) + c_0} < d_{\max}.$$

1197 **(3) Finite fixed point and monotone convergence for  $d_* < d_{\max}$ .** By (2),  $F(\cdot)$  is continuous,  
1198 strictly increasing, with range  $(0, d_{\max})$ . Therefore, there exists a unique  $\mu^* \in \mathbb{R}$  such that  $F(\mu^*) =$   
1199  $d_*$ . Now we first argue  $\mu(t) \rightarrow \mu^*$ .

1200 Consider the ODE  $\dot{\mu} = c(d_* - F(\mu))$  with  $c = \alpha/(n\sqrt{K}) > 0$ . If  $\mu(0) = 0 \leq \mu^*$  and (thus)  
1201  $F(\mu(0)) \leq F(\mu^*) = d_*$ , then  $\dot{\mu}(t) \geq 0$  as long as  $\mu(t) \leq \mu^*$ , hence  $\mu$  is non-decreasing and  
1202 bounded above by  $\mu^*$ ; monotone convergence implies  $\mu(t) \rightarrow \bar{\mu} \leq \mu^*$  for some  $\bar{\mu}$ . By the continuity  
1203 of  $F(\cdot)$  and the fact that  $\dot{\mu} \rightarrow 0$ , we can obtain that  $F(\bar{\mu}) = d_*$ , which implies  $\bar{\mu} = \mu^*$ . The case  
1204  $\mu(0) > \mu^*$  is analogous with a non-increasing trajectory.

1205 For local exponential stability, we can set  $\tilde{\mu} = \mu - \mu^*$  and write

$$1207 \dot{\tilde{\mu}}(t) = -c(F(\mu^* + \tilde{\mu}(t)) - F(\mu^*)).$$

1209 By the mean value theorem,  $F(\mu^* + \tilde{\mu}) - F(\mu^*) = F'(\xi) \tilde{\mu}$  for some  $\xi$  between  $\mu^*$  and  $\mu^* + \tilde{\mu}$ . Since  
1210  $F'(\mu^*) > 0$  and  $F'$  is continuous, there exists  $\eta > 0$  and  $m > 0$  such that  $F'(\xi) \geq m$  whenever  
1211  $|\xi - \mu^*| \leq \eta$ . Hence, as long as  $|\tilde{\mu}(t)| \leq \eta$ , we have

$$1212 \frac{d}{dt} |\tilde{\mu}(t)| = \frac{\tilde{\mu}(t)}{|\tilde{\mu}(t)|} \dot{\tilde{\mu}}(t) = -c F'(\xi(t)) |\tilde{\mu}(t)| \leq -c m |\tilde{\mu}(t)|.$$

1214 Applying Gronwall's inequality, we have  $|\tilde{\mu}(t)| \leq e^{-cmt} |\tilde{\mu}(0)|$  in this neighborhood, which estab-  
1215 lishes local exponential convergence.

1217 **(4) Divergence and logarithmic lower bound for  $d_* = d_{\max}$ .** When  $d_* = d_{\max}$ , since  $F(\mu) <$   
1218  $d_{\max}$  for all finite  $\mu$ , we have  $\dot{\mu}(t) = c(d_{\max} - F(\mu(t))) > 0$  where  $c = \frac{\alpha}{n\sqrt{K}}$  and thus  $\mu(t)$  is  
1219 strictly increasing. We now lower bound the growth rate similar to Lemma 5.

1220 Since  $S(\mu) \leq d_{\max} E_+(\mu)$ , we have

$$1222 d_{\max} - F(\mu) = d_{\max} - \frac{S(\mu)}{E_+(\mu) + c_0} \geq d_{\max} \left(1 - \frac{E_+(\mu)}{E_+(\mu) + c_0}\right) = \frac{d_{\max} c_0}{E_+(\mu) + c_0}.$$

1224 Moreover, for each  $u \in \mathcal{N}_{c+1}$ , it holds that

$$1226 e^{\xi_u(\mu)} \leq \exp(\lambda(1 + \mu d_{\max})).$$

1227 Therefore,  $E_+(\mu) \leq |\mathcal{N}_{c+1}| e^{\lambda(1 + \mu d_{\max})} \leq n e^{\lambda(1 + \mu d_{\max})}$  and thus we can obtain that

$$1229 E_+(\mu) + c_0 \leq n e^{\lambda(1 + \mu d_{\max})} + c_0 \leq n (e^{\lambda(1 + \mu d_{\max})} + 1) \leq 2n e^{\lambda(1 + \mu d_{\max})},$$

1231 where we used  $e^x \geq 1$  for  $x \geq 0$ . Combining the above derivation, we can obtain that

$$1232 d_{\max} - F(\mu) \geq \frac{d_{\max} c_0}{2n} e^{-\lambda} e^{-\lambda d_{\max} \mu}.$$

1234 We can then plug this into  $\dot{\mu} = c(d_{\max} - F(\mu))$  with  $c = \alpha/(n\sqrt{K})$  to get

$$1236 \dot{\mu}(t) \geq \frac{\alpha}{n\sqrt{K}} \cdot \frac{d_{\max} c_0}{2n} e^{-\lambda} e^{-\lambda d_{\max} \mu(t)} = c_1 e^{-c_2 \mu(t)},$$

1238 where  $c_1 = \frac{\alpha d_{\max} c_0 e^{-\lambda}}{2n^2 \sqrt{K}}$  and  $c_2 = \lambda d_{\max} > 0$ .

1241 Applying Lemma 13, we can obtain exactly (13). This shows  $\mu(t) \rightarrow +\infty$  at least logarithmically  
1242 fast.  $\square$

1242 B.3 THOUGHT EXPANSION  
12431244 Finally, we provide results for continuous thought expansion. Note that the following results hold  
1245 for any directed graph that differs from the graphs in the training set.1246 **Theorem 5** (One-hop expansion of continuous thoughts). *Let  $\mathcal{G} = (\mathcal{V}, \mathcal{E})$  be any directed graph  
1247 (which can differ from the graphs in the training set) and  $x \in \mathcal{V}$  be a root node. Assume the current  
1248 thought is any positive superposition on  $\mathcal{N}_c^{\mathcal{G}}(x)$ :*

1249 
$$\mathbf{h}_{[\mathbf{t}_c]} = \sum_{u \in \mathcal{N}_c} \lambda_u \mathbf{E}(u), \quad \lambda_u > 0.$$
  
1250  
1251

1252 Then the next continuous thought  $[\mathbf{t}_{c+1}] = \mathbf{h}_{[\mathbf{t}_{c+1}]}$  generated by the forward pass (2) satisfies  
1253

1254 
$$\boldsymbol{\xi} = \mathbf{U}^{\top} \mathbf{h}_{[\mathbf{t}_{c+1}]} = \sum_{v \in \mathcal{N}_{c+1}} \beta_v \mathbf{e}_v,$$
  
1255

1256 with coefficients  
1257

1258 
$$\beta_v = \underbrace{\lambda_v \mathbb{1}\{v \in \mathcal{N}_c\}}_{\text{carryover}} + \underbrace{\mu \sum_{u \in \mathcal{N}_c} \lambda_u \mathbb{1}\{(u \rightarrow v) \in \mathcal{E}\}}_{\text{one-hop expansion}} \geq 0. \quad (14)$$
  
1259  
1260  
1261

1262 where we assume the model has been trained until time  $t$  and the trained model satisfies  $\mu_v(t) \equiv$   
1263  $\mu > 0$  in (3). In particular,  $\beta_v > 0$  for every  $v \in \mathcal{N}_{c+1}$  if  $\mu > 0$ , so the support of  $\boldsymbol{\xi}$  is exactly  $\mathcal{N}_{c+1}$ ,  
1264 and the output is a superposition of  $\mathcal{N}_{c+1}$ .  
12651266 *Proof.* Note that  $\mathbf{h}_i = \mathbf{E}_s(s_i) + \mathbf{E}_t(t_i)$  and  $\mathbf{W} = \sum_{v \in \mathcal{V}} \mu_v(t) \mathbf{E}(v) \mathbf{E}_s(v)^{\top} = \sum_{v \in \mathcal{V}} \mu \mathbf{E}(v) \mathbf{E}_s(v)^{\top}$ .  
1267 We can calculate that

1268 
$$\mathbf{W} \mathbf{h}_i = \sum_{v \in \mathcal{V}} \mu \mathbf{E}(v) \mathbf{E}_s(v)^{\top} (\mathbf{E}_s(s_i) + \mathbf{E}_t(t_i)) = \mu \mathbf{E}(s_i),$$
  
1269  
1270

1271 where we used  $\mathbf{E}_s(v)^{\top} \mathbf{E}_s(s_i) = \mathbb{1}\{v = s_i\}$  and  $\mathbf{E}_s(v)^{\top} \mathbf{E}_t(t_i) = 0$  according to Assumption 1.  
1272 Therefore, with  $\mathbf{h}_{[\mathbf{t}_c]} = \sum_{u \in \mathcal{N}_c} \lambda_u \mathbf{E}(u)$ , we can calculate

1273 
$$\alpha_i := \mathbf{h}_{[\mathbf{t}_c]}^{\top} \mathbf{W} \mathbf{h}_i = \mu \sum_{u \in \mathcal{N}_c} \lambda_u \mathbf{E}(u)^{\top} \mathbf{E}(s_i) = \mu \lambda_{s_i} \mathbb{1}\{s_i \in \mathcal{N}_c\}.$$
  
1274  
1275

1276 The value aggregation becomes  
1277

1278 
$$\phi(\mathbf{h}_{[\mathbf{t}_c]}; \{\mathbf{h}_i\}) = \sum_{i=1}^m \alpha_i \mathbf{h}_i = \mu \sum_{i: s_i \in \mathcal{N}_c} \lambda_{s_i} (\mathbf{E}_s(s_i) + \mathbf{E}_t(t_i)).$$
  
1279  
1280

1281 Furthermore, we have

1282 
$$\mathbf{U}^{\top} \phi(\mathbf{h}_{[\mathbf{t}_c]}; \{\mathbf{h}_i\}) = \mu \sum_{i: s_i \in \mathcal{N}_c} \lambda_{s_i} \mathbf{e}_{t_i} = \mu \sum_{v \in \mathcal{V}} \left( \sum_{u \in \mathcal{N}_c} \lambda_u \mathbb{1}\{(u \rightarrow v) \in \mathcal{E}\} \right) \mathbf{e}_v.$$
  
1283  
1284

1285 Similarly,

1286 
$$\mathbf{U}^{\top} \mathbf{h}_{[\mathbf{t}_c]} = \sum_{v \in \mathcal{N}_c} \lambda_v \mathbf{e}_v = \sum_{v \in \mathcal{V}} \lambda_v \mathbb{1}\{v \in \mathcal{N}_c\} \mathbf{e}_v.$$
  
1287

1288 Adding the two parts yields  $\boldsymbol{\xi} = \sum_v \beta_v \mathbf{e}_v$  with  $\beta_v$  as in (14), since by definition we have  $\mathbf{h}_{[\mathbf{t}_{c+1}]} =$   
1289  $\mathbf{h}_{[\mathbf{t}_c]} + \phi(\mathbf{h}_{[\mathbf{t}_c]}; \{\mathbf{h}_i\})$  and  $\boldsymbol{\xi} = \mathbf{U}^{\top} \mathbf{h}_{[\mathbf{t}_{c+1}]}$ .  $\square$   
12901291 C MISSING PROOFS FOR SECTION 4  
12921293 In this section, we analyze the training dynamics of the prediction stage, i.e., after thought gener-  
1294 ation, how the model extracts the information from the generated continuous thought to make the  
1295 final prediction.

Recall that the  $i$ -th training sample consists of  $(\mathcal{G}^{(i)}, \mathbf{r}^{(i)}, \mathbf{c}_1^{(i)}, \mathbf{c}_2^{(i)}, \boldsymbol{\lambda}^{(i)})$ , and we denote  $\mathbf{c}_\star^{(i)}$  as the reachable candidate and  $\mathbf{c}_\perp^{(i)}$  as the unreachable candidate. We also use  $\mathcal{N}_C^{(i)} = \mathcal{N}_C^{\mathcal{G}^{(i)}}(\mathbf{r}^{(i)})$  to denote the  $C$ -ball for the  $i$ -th training sample. We assume  $C$  is large enough so that  $\mathbf{c}_\star^{(i)} \in \mathcal{N}_C^{(i)}$  for any  $i$ . Note that  $\mathbf{c}_\perp^{(i)} \notin \mathcal{N}_C^{(i)}$  for any  $C$  by definition. For notation convenience, we also use  $\mu_A = \mu_{\langle A \rangle}$ ,  $\mu_R = \mu_{\langle R \rangle}$ , and denote  $\boldsymbol{\xi}^{(i)} = \{\xi_v^{(i)}\}_{v \in \mathcal{V}_{\text{oc}}}$  as the logits calculated by forward pass (7) for the  $i$ -th training sample. We denote  $\xi_{\mathbf{c}_t^{(i)}}^{(i)} = \xi_{\mathbf{c}_t}^{(i)}$ ,  $\lambda_{\mathbf{c}_t^{(i)}}^{(i)} = \lambda_{\mathbf{c}_t}^{(i)}$  for  $t \in \{1, 2, \star, \perp\}$  for notation convenience.

To start with, we first provide a closed-form logit expression.

**Lemma 8** (Closed-form logits in prediction stage). *Under reparameterization (8) and forward pass for the prediction stage (7), for every  $v \in \mathcal{V}$  we have*

$$\xi_v(\mu_{\langle A \rangle}, \mu_{\langle R \rangle}) = \underbrace{\mu_{\langle A \rangle} \lambda_v}_{\text{frontier residual}} + \underbrace{\mu_{\langle R \rangle} \mathbb{1}\{v \in \{\mathbf{c}_1, \mathbf{c}_2\}\}}_{\text{candidate lift}}. \quad (15)$$

In particular,

$$\xi_{\mathbf{c}_\star} - \xi_{\mathbf{c}_\perp} = \mu_{\langle A \rangle} \lambda_{\mathbf{c}_\star}. \quad (16)$$

*Proof.* For the reasoning token  $\mathbf{h}_{\text{Idx}(\langle R \rangle)} = \mathbf{E}(\langle R \rangle) + \mathbf{E}(\mathbf{c}_1) + \mathbf{E}(\mathbf{c}_2)$ , we have

$$\mathbf{W}\mathbf{h}_{\text{Idx}(\langle R \rangle)} = \mu_{\langle R \rangle} \mathbf{E}(\langle A \rangle) \underbrace{\mathbf{E}(\langle R \rangle)^\top \mathbf{h}_{\text{Idx}(\langle R \rangle)}}_{=1} = \mu_{\langle R \rangle} \mathbf{E}(\langle A \rangle).$$

Therefore,

$$\mathbf{U}^\top((\mathbf{h}_{\text{Idx}(\langle A \rangle)}^\top \mathbf{W}\mathbf{h}_{\text{Idx}(\langle R \rangle)}) \mathbf{h}_{\text{Idx}(\langle R \rangle)}) = \mu_{\langle R \rangle} (\mathbf{e}_{\langle R \rangle} + \mathbf{e}_{\mathbf{c}_1} + \mathbf{e}_{\mathbf{c}_2}).$$

Also,

$$\mathbf{U}^\top(\mu_{\langle A \rangle} \mathbf{h}_{\text{Idx}(\langle A \rangle)}) = \mu_{\langle A \rangle} \sum_{u \in \mathcal{N}_C} \lambda_u \mathbf{e}_u + \mu_{\langle A \rangle} \mathbf{e}_{\langle A \rangle}.$$

Combining the above two expressions yields (15). For  $\mathbf{c}_\perp \notin \mathcal{N}_C$  we have  $\lambda_{\mathbf{c}_\perp} = 0$ , and (16) follows.  $\square$

For each training sample, we can construct a two-dimensional feature for every node  $v \in \mathcal{V}$ :

$$\mathbf{x}_v^{(i)} := (\lambda_v^{(i)}, \mathbb{1}\{v \in \{\mathbf{c}_1^{(i)}, \mathbf{c}_2^{(i)}\}\}) \in \mathbb{R}_{\geq 0}^2,$$

so that  $\xi_v^{(i)}(\mu_A, \mu_R) = \langle \mathbf{w}, \mathbf{x}_v^{(i)} \rangle$  with  $\mathbf{w} := (\mu_A, \mu_R) \in \mathbb{R}_{\geq 0}^2$ . For instance  $i$ , a correct classification means  $\langle \mathbf{w}, \mathbf{x}_{\mathbf{c}_\star}^{(i)} - \mathbf{x}_v^{(i)} \rangle > 0$  for all  $v \neq \mathbf{c}_\star^{(i)}$ , where we denote  $\mathbf{x}_{\mathbf{c}_t^{(i)}}^{(i)} = \mathbf{x}_{\mathbf{c}_t}^{(i)}$  for  $t \in \{1, 2, \star, \perp\}$ . We further define the difference of features with respect to  $\mathbf{c}_\star$  for later use:

$$\Delta_{i,v} := \mathbf{x}_{\mathbf{c}_\star}^{(i)} - \mathbf{x}_v^{(i)} = \begin{cases} (\lambda_{\mathbf{c}_\star}^{(i)}, 0), & v = \mathbf{c}_\perp^{(i)}, \\ (\lambda_{\mathbf{c}_\star}^{(i)} - \lambda_v^{(i)}, 1), & v \in \mathcal{N}_C^{(i)} \setminus \{\mathbf{c}_\star^{(i)}\}, \\ (\lambda_{\mathbf{c}_\star}^{(i)}, 1), & v \notin \mathcal{N}_C^{(i)} \cup \{\mathbf{c}_\perp^{(i)}\}. \end{cases} \quad (17)$$

### C.1 LINEARLY SEPARABLE STRUCTURE AND A MAX-MARGIN PROBLEM

**Lemma 9** (Separation by a nonnegative direction). *For every instance  $i$  and each competitor  $v \neq \mathbf{c}_\star^{(i)}$ ,*

$$\langle (1, 1), \Delta_{i,v} \rangle = \begin{cases} \lambda_{\mathbf{c}_\star}^{(i)}, & v = \mathbf{c}_\perp^{(i)}, \\ \lambda_{\mathbf{c}_\star}^{(i)} - \lambda_v^{(i)} + 1, & v \in \mathcal{N}_C^{(i)} \setminus \{\mathbf{c}_\star^{(i)}\}, \\ \lambda_{\mathbf{c}_\star}^{(i)} + 1, & v \notin \mathcal{N}_C^{(i)} \cup \{\mathbf{c}_\perp^{(i)}\}, \end{cases} > 0.$$

Hence, the training data are linearly separable by a direction in  $\mathbb{R}_{\geq 0}^2$ .

*Proof.* The result holds because  $\lambda_{\mathbf{c}_\star}^{(i)} > 0$ ,  $\lambda_v^{(i)} \leq 1$ .  $\square$

1350 Define the *hard-margin* value of a unit direction  $u \in \mathbb{S}^1 \cap \mathbb{R}_{\geq 0}^2$  (where  $\mathbb{S}^1 = \{u \in \mathbb{R}^2 : \|u\|_2 = 1\}$ )  
 1351 as

$$1352 \quad \gamma(u) := \min_i \min_{v \neq c_*^{(i)}} \langle u, \Delta_{i,v} \rangle.$$

1354 The corresponding *maximum-margin* direction is

$$1355 \quad u^* \in \arg \max_{u \in \mathbb{S}^1 \cap \mathbb{R}_{\geq 0}^2} \gamma(u). \quad (18)$$

1357 We characterize  $u^*$  using the following two quantities of the training sets:

$$1358 \quad \lambda_* := \min_i \lambda_{c_*}^{(i)} \in (0, 1], \quad \Delta_{\text{train}} := \max_i \max_{v \in \mathcal{N}_C^{(i)} \setminus \{c_*^{(i)}\}} (\lambda_v^{(i)} - \lambda_{c_*}^{(i)})_+ \in [0, 1],$$

1360 where  $(x)_+ := \max\{x, 0\}$ . Intuitively,  $\lambda_*$  is the smallest mass ever placed on a reachable candidate  
 1361 across the training set, and  $\Delta_{\text{train}}$  is the largest overshoot of a non-candidate but reachable node's  
 1362 weight relative to the reachable candidate.

1363 **Lemma 10** (Closed-form lower envelope of the margin). *For any unit  $u = (u_A, u_R) \in \mathbb{S}^1 \cap \mathbb{R}_{\geq 0}^2$ ,*

$$1364 \quad \gamma(u) = \min \{u_A \lambda_*, u_R - u_A \Delta_{\text{train}}, u_A \lambda_* + u_R\} = \min \{u_A \lambda_*, u_R - u_A \Delta_{\text{train}}\}.$$

1366 *Proof.* According to (17), we can directly obtain the the lower bounds  $u_A \lambda_{c_*}^{(i)}$ ,  $u_R + u_A (\lambda_{c_*}^{(i)} - \lambda_v^{(i)})$ ,  
 1367 and  $u_A \lambda_{c_*}^{(i)} + u_R$ . Minimizing over  $i$  and  $v$  according to the definition of  $\lambda_*$ ,  $\Delta_{\text{train}}$  yields the desired  
 1368 result.  $\square$

1370 **Proposition C.1** (Properties of the maximum-margin direction). *Let  $u^* = (u_A^*, u_R^*)$  be a solution  
 1371 of (18). Then the unique maximizer satisfies*

$$1372 \quad \frac{u_R^*}{u_A^*} = \lambda_* + \Delta_{\text{train}}, \quad u_A^* = \frac{1}{\sqrt{1 + (\lambda_* + \Delta_{\text{train}})^2}}, \quad u_R^* = \frac{\lambda_* + \Delta_{\text{train}}}{\sqrt{1 + (\lambda_* + \Delta_{\text{train}})^2}}.$$

1375 *Proof.* By Lemma 10, we can maximize  $\gamma(u) = \min \{u_A \lambda_*, u_R - u_A \Delta_{\text{train}}\}$  over the unit vector  $u$   
 1376 by equalizing the two arguments (otherwise one can rotate  $u$  to increase the minimum). Therefore,  
 1377 we can equalize the two arguments, which yields  $u_R = u_A (\lambda_* + \Delta_{\text{train}})$ , and obtain the desired  
 1378 result.  $\square$

## 1380 C.2 IMPLICIT BIAS OF GRADIENT FLOW AND DIRECTIONAL CONVERGENCE

$$1382 \quad \ell_{\mathcal{G}, \mathbf{r}, \mathbf{c}_1, \mathbf{c}_2, \boldsymbol{\lambda}}^{\text{pred}} := -\log \frac{\exp(\xi_{c_*})}{\sum_{v \in \mathcal{V}} \exp(\xi_v)}, \quad \mathcal{L}^{\text{pred}} = \mathbb{E}_{(\mathcal{G}, \mathbf{r}, \mathbf{c}_1, \mathbf{c}_2, \boldsymbol{\lambda}) \sim \mathcal{D}} [\ell_{\mathcal{G}, \mathbf{r}, \mathbf{c}_1, \mathbf{c}_2, \boldsymbol{\lambda}}^{\text{pred}}],$$

1384 Recall the loss function on the prediction stage over the training set (9). We can rewrite it as follows

$$1386 \quad \mathcal{L}(\mu_A, \mu_R) := \frac{1}{N} \sum_{i=1}^N \ell^{(i)}(\mu_A, \mu_R), \quad \ell^{(i)}(\mu_A, \mu_R) := -\log \frac{\exp(\xi_{c_*^{(i)}}^{(i)})}{\sum_{v \in \mathcal{V}} \exp(\xi_v^{(i)})},$$

1388 and run the gradient-flow dynamics  $\dot{w}(t) = -\alpha \nabla \mathcal{L}(w(t))$  with  $w(t) = (\mu_A(t), \mu_R(t))$  and  $\alpha > 0$ .  
 1389 By Lemma 9, the data are linearly separable, so the implicit bias of gradient flow directly yields the  
 1390 following lemma.

1391 **Lemma 11** (Implicit bias of gradient flow). *Along gradient flow from any bounded initialization  
 1392  $w(0)$ , we have*

$$1394 \quad \|w(t)\| \rightarrow \infty, \quad \frac{w(t)}{\|w(t)\|} \rightarrow u^*,$$

1395 where  $u^*$  is the unique solution to the maximum-margin problem (18). Combining Proposition C.1,  
 1396 there exists a scalar radius  $r(t) \rightarrow \infty$  such that

$$1398 \quad (\mu_A(t), \mu_R(t)) = r(t) u^* + o(r(t)),$$

1399 and for any  $\varepsilon > 0$ ,

$$1400 \quad \frac{\mu_R(t)}{\mu_A(t)} \geq \lambda_* + \Delta_{\text{train}} - \varepsilon \quad \text{for all sufficiently large } t.$$

1402 The proof can be straightforwardly adapted from its gradient descent counterpart (Soudry et al.,  
 1403 2018).

1404 C.3 PREDICTION ON UNSEEN GRAPHS  
14051406 Finally, we show that after sufficient training, the model can correctly predict the reachable candidate  
1407 node even for unseen graphs, showcasing its generalization capability.1408 Fix any unseen test graph along with the exploration set  $\mathcal{N}_C^{\text{test}}$  and weights  $\lambda^{\text{test}}$ , such that  $\lambda_v^{\text{test}} \in$   
1409  $(0, 1]$  on  $\mathcal{N}_C^{\text{test}}$  and 0 otherwise. The test graph also satisfies  
1410

1411 
$$\max_{u \in \mathcal{N}_C^{\text{test}}} \lambda_u^{\text{test}} - \lambda_{c_*}^{\text{test}} \leq \Delta, \quad \text{with } \Delta \leq \Delta_{\text{train}}.$$
  
1412

1413 Therefore, for every non-candidate  $v \in \mathcal{N}_C^{\text{test}} \setminus \{c_*^{\text{test}}\}$ , it holds that  $\lambda_v^{\text{test}} \leq \lambda_{c_*}^{\text{test}} + \Delta$ .  
14141415 The following lemma shows that as long as the test graph satisfies the above condition, it has a  
1416 positive margin using the maximum margin direction for the training set  $u^*$ .  
14171418 **Lemma 12** (Positive test-time margins from the trained direction). *Let  $u^* = (u_A^*, u_R^*)$  be the unique  
1419 max-margin direction with  $u_R^*/u_A^* = \lambda_* + \Delta_{\text{train}} > \Delta$ . Then for every competitor  $v \neq c_*^{\text{test}}$ ,*  
1420

1421 
$$\langle u^*, x_{c_*}^{\text{test}} - x_v^{\text{test}} \rangle \geq \min\{u_A^* \lambda_*, u_A^* \lambda_*^{\text{test}}\} > 0.$$
  
1422

1423 *Proof.* For  $v = c_\perp^{\text{test}}$ , the difference is  $(\lambda_{c_*}^{\text{test}}, 0)$ ; since  $\lambda_{c_*}^{\text{test}} > 0$  we have  $\langle u^*, x_{c_*}^{\text{test}} - x_{c_\perp}^{\text{test}} \rangle \geq$   
1424  $u_A^* \lambda_{c_*}^{\text{test}} > 0$ .1425 For  $v \notin \mathcal{N}_C^{\text{test}}$  the difference is  $(\lambda_{c_*}^{\text{test}}, 1)$  and the bound is even larger.  
14261427 For  $v \in \mathcal{N}_C^{\text{test}} \setminus \{c_*^{\text{test}}\}$ , we have  $\lambda_v^{\text{test}} \leq \lambda_{c_*}^{\text{test}} + \Delta$ , hence  
1428

1429 
$$\langle u^*, x_{c_*}^{\text{test}} - x_v^{\text{test}} \rangle = u_A^* (\lambda_{c_*}^{\text{test}} - \lambda_v^{\text{test}}) + u_R^* \geq u_R^* - u_A^* \Delta \geq u_A^* (\lambda_* + \Delta_{\text{train}} - \Delta) \geq u_A^* \lambda_* > 0.$$
  
1430

□

1431  
1432 Finally, we show that after sufficient training, the model can correctly predict the reachable candidate  
1433 node .  
14341435 **Theorem 6** (Generalization for unseen graphs). *Let  $(\mu_A(t), \mu_R(t))$  follow gradient flow on the loss  
1436 (9) from any bounded initialization. Suppose the training set is linearly separable and  $\lambda_*$ ,  $\Delta_{\text{train}}$  are  
1437 defined as above. Then, for any unseen instance satisfying  $\lambda_v^{\text{test}} \in (0, 1]$  on  $\mathcal{N}_C^{\text{test}}$  and 0 otherwise,  
1438 and  
1439*

1440 
$$\max_{u \in \mathcal{N}_C^{\text{test}}} \lambda_u^{\text{test}} - \lambda_{c_*}^{\text{test}} \leq \Delta, \quad \text{with } \Delta \leq \Delta_{\text{train}},$$
  
1441

1442 we have for all sufficiently large  $t$ :

1443  
1444 
$$p_{c_*^{\text{test}}}(t) := \frac{\exp(\xi_{c_*}^{\text{test}}(\mu_A(t), \mu_R(t)))}{\sum_v \exp(\xi_v^{\text{test}}(\mu_A(t), \mu_R(t)))} \rightarrow 1.$$
  
1445

1446  
1447 *Proof.* By Lemma 11, we have  
1448

1449 
$$(\mu_A(t), \mu_R(t)) = r(t)u^* + o(r(t)), \quad r(t) \rightarrow \infty.$$
  
1450

1451 Then, by Lemma 12, for every competitor  $v \neq c_*^{\text{test}}$ ,  
1452

1453 
$$\begin{aligned} & \xi_{c_*}^{\text{test}}(\mu_A(t), \mu_R(t)) - \xi_v^{\text{test}}(\mu_A(t), \mu_R(t)) \\ &= r(t) \langle u^*, x_{c_*}^{\text{test}} - x_v^{\text{test}} \rangle + o(r(t)) \\ &\geq r(t) \cdot \min\{u_A^* \lambda_*, u_A^* \lambda_*^{\text{test}}\} + o(r(t)) \xrightarrow[t \rightarrow \infty]{} +\infty. \end{aligned}$$
  
1454

1455  
1456 Hence the arg max is  $c_*^{\text{test}}$ , and its softmax probability tends to 1.  
1457 □

1458 **D AUXILIARY LEMMAS**  
14591460 **Lemma 13** (ODE lower bound). *Let  $c_1, c_2 > 0$  be two constants. Assume the function  $f : \mathbb{R} \rightarrow \mathbb{R}$   
1461 satisfies  $f(0) = 0$  and*

1462 
$$\frac{df(t)}{dt} \geq c_1 \cdot \exp(-c_2 \cdot f(t)), \quad \forall t \geq 0.$$
  
1463

1464 *Then it holds*

1465 
$$f(t) \geq \frac{1}{c_2} \ln(1 + c_1 c_2 t)$$
  
1466

1467 *for all  $t \geq 0$ .*  
14681469 *Proof.* We define  $g(t) = e^{c_2 f(t)}$ . Note that  
1470

1471 
$$\frac{dg(t)}{dt} = \frac{d}{dt}(e^{c_2 f(t)}) = c_2 \frac{df(t)}{dt} \cdot e^{c_2 f(t)} \geq c_2 \cdot c_1 \cdot \exp(-c_2 \cdot f(t)) \exp(c_2 f(t)) = c_1 c_2.$$
  
1472

1473 Therefore,  $dg(t) \geq c_1 c_2 dt$  for  $t \geq 0$ , and thus  
1474

1475 
$$\int_0^t dg(t) \geq \int_0^t c_1 c_2 dt \implies g(t) - g(0) \geq c_1 c_2 t.$$
  
1476

1477 Therefore,  
1478

1479 
$$g(t) = e^{c_2 f(t)} \geq g(0) + c_1 c_2 t = e^{c_2 f(0)} + c_1 c_2 t = 1 + c_1 c_2 t,$$
  
1480

1481 which implies  
1482

1483 
$$f(t) \geq \frac{1}{c_2} \ln(1 + c_1 c_2 t).$$
  
1484

1485  $\square$   
14861487 **E EXPERIMENT DETAILS**  
14881489 **E.1 DATASET**  
14901491 Table 3: ProsQA statistics. Numbers are averaged over problem instances.  
1492

	#Problems	$ V $	$ E $	Sol. Len.
Train	14785	22.8	36.5	3.5
Val	257	22.7	36.3	3.5
Test	419	22.7	36.0	3.5

1493 The statistics of the ProsQA dataset is shown in Table 3.  
14941495 **E.2 EXPERIMENT WITH COCONUT-BFS**  
14961497 As a comparison, we also train a model with a modified version of  $\mathcal{L}^{\text{BFS}}$ . Recall that the original  
1498  $\mathcal{L}^{\text{BFS}}$  (5) encourages the model to predict any nodes within  $\mathcal{N}_{c+1}$ . To avoid the trivial solution of al-  
1499 ways predicting the root node, we introduce an experimental variant that only encourages predicting  
1500 nodes on the current frontier:  
1501

1502 **COCONUT-BFS-exp:**  $\ell_{\mathcal{G}, r}^{\text{BFS-exp}} := -\log \frac{\sum_{v \in \mathcal{N}_{c+1} \setminus \mathcal{N}_c} \exp(\xi_v)}{\sum_{v \in \mathcal{V}} \exp(\xi_v)}.$  (19)  
1503

1504 All other training settings remain unchanged. The answer accuracy of this model on the test set is  
1505 99.0%. We then track the logit difference between frontier and non-frontier edges as a proxy for  $\mu_v$ ,  
1506 with results shown in Figure 5.  
1507

Number of layers		Number of heads		Width	
$L = 2$	98.8	$H = 4$	98.0	$d_{\text{model}} = 384$	62.0
$L = 4$	97.3	$H = 8$	98.8	$d_{\text{model}} = 768$	98.8
$L = 8$	96.5	$H = 12$	98.8	$d_{\text{model}} = 1536$	97.7
$L = 12$	67.4				

Learning rate		Weight tying	
$\eta = 2 \times 10^{-4}$	58.1	Tied	98.8
$\eta = 1 \times 10^{-4}$	98.8	Untied	98.8
$\eta = 5 \times 10^{-5}$	62.1		

Table 4: Ablation on depth, heads, width, learning rate, and weight tying. By default, other hyper-parameters follow the main experiments.

In Stage 1, the logit difference for  $c = 1$  grows much faster than under  $\mathcal{L}^{\text{coco}}$  and shows no sign of saturation even after 150 epochs. This agrees with the theoretical prediction in Theorem 1: under COCONUT-BFS,  $\mu_v$  diverges rather than stabilizing. At later steps ( $c = 3, 4$ ), the gap between COCONUT-BFS and COCONUT becomes smaller. We attribute this to practical factors such as stage-wise data mixing, gradient propagation across earlier thoughts, and a larger discrepancy between losses (5) and (19) in the later stage.

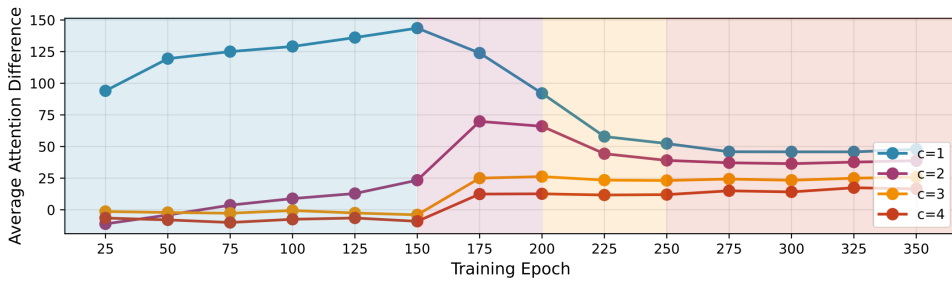


Figure 5: The attention logits difference between frontier edges and others. The model is trained with a modified version of  $\mathcal{L}^{\text{BFS}}$ .

### E.3 ALTERNATIVE ATTENTION ROUTES FOR CANDIDATE LIFT

Our theoretical analysis in Lemma 2 assumes that  $\langle R \rangle$  copies the candidate nodes in the first layer, and  $\langle A \rangle$  then attends to  $\langle R \rangle$  in the second layer. In practice, however, we observe three distinct yet functionally equivalent attention routes that realize the same *candidate lift*. Example attention maps for each route are shown in Figure 6.

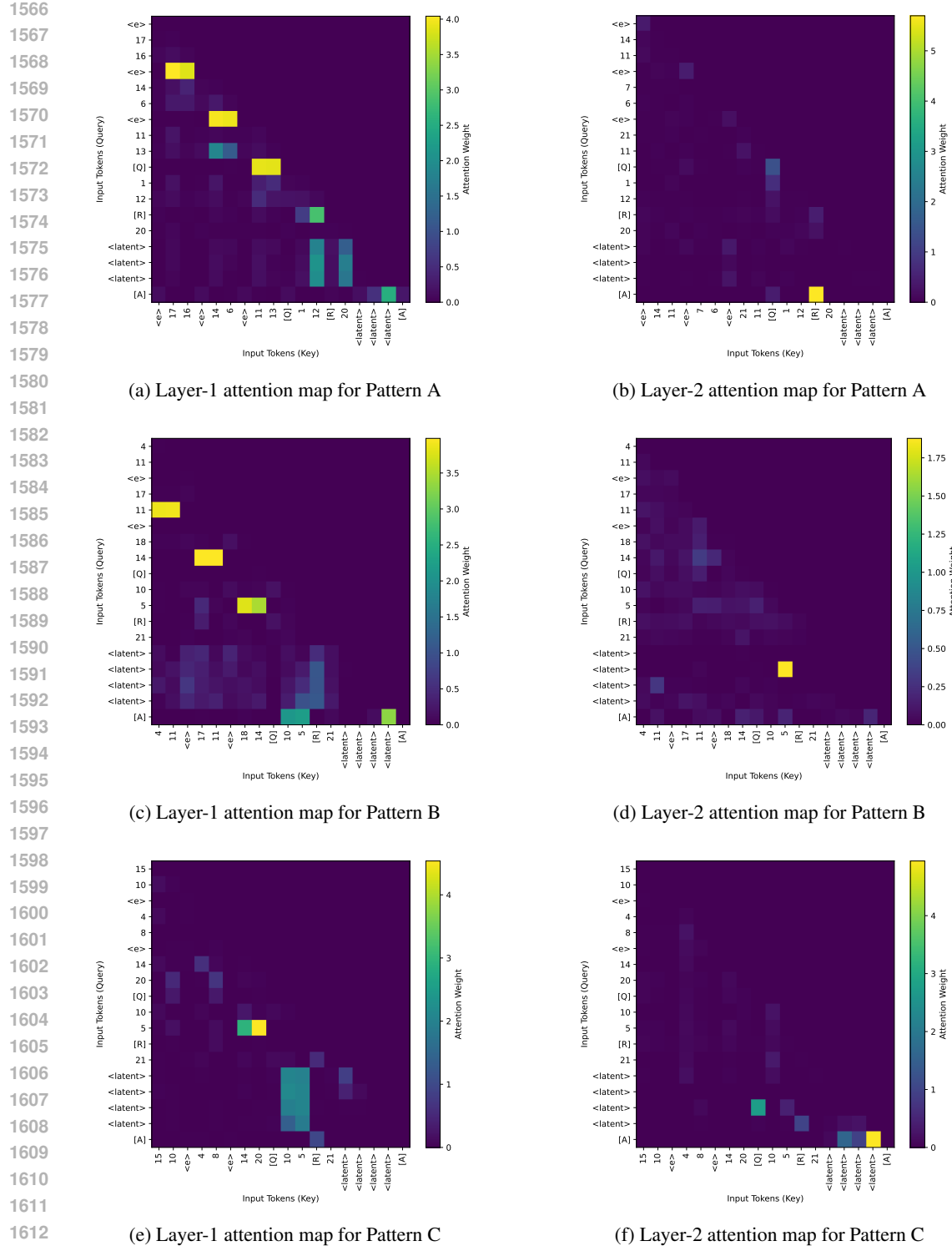
## F ADDITIONAL EXPERIMENTAL RESULTS

In this section, we provide additional experiments to complement our main analysis of training dynamics.

### F.1 ABLATION STUDY: ARCHITECTURAL AND OPTIMIZATION SENSITIVITY

We evaluate the sensitivity of COCONUT training to model depth, number of attention heads, hidden width, and learning rate. The results are summarized in Table 4.

We observe that models with  $L = \{4, 8\}$  layers maintain high accuracy, while  $L = 12$  is harder to optimize. The performance remains comparable when  $d_{\text{model}} \in \{768, 1536\}$ , but degrades when the width is too small (e.g.,  $d_{\text{model}} = 384$ ). Varying the number of heads does not have major effects on



1614  
1615  
1616  
1617  
1618  
1619

Figure 6: Example attention maps illustrating three alternative routes for *candidate lift*. For clarity, we omit earlier tokens in the sequence and only visualize the final segment containing some of edges, the candidate nodes, latent thoughts, and answer tokens. **Pattern A** (consistent with the theoretical assumption):  $\langle R \rangle$  copies candidate nodes in Layer 1, and  $\langle A \rangle$  attends to  $\langle R \rangle$  in Layer 2. **Pattern B**:  $\langle A \rangle$  directly attends to candidate nodes in Layer 1. **Pattern C**: continuous thoughts copy candidate nodes in Layer 1, and  $\langle A \rangle$  attends to the continuous thoughts in Layer 2. All three patterns achieve the same functional effect of lifting the reachable candidate.

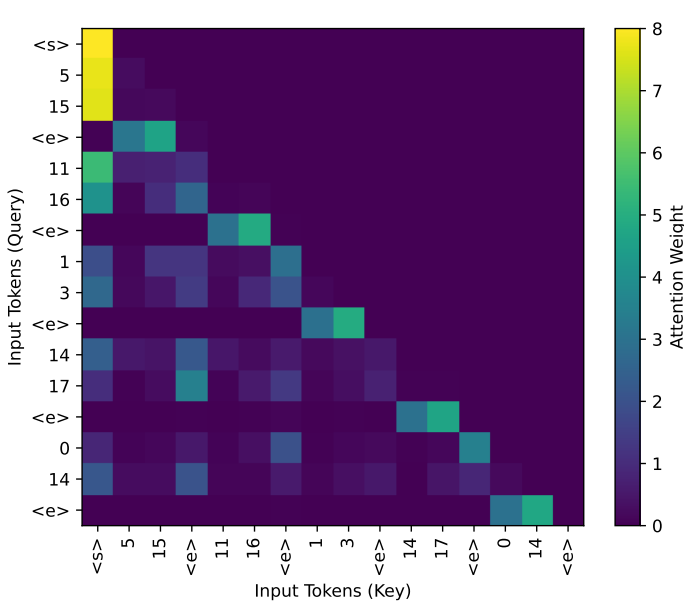


Figure 7: The first-layer attention patterns in 4-layer transformers.  $<e>$  tokens attend to the corresponding source and target nodes to aggregate the information. This is consistent with the analysis of the two-layer transformer in Zhu et al. (2025).

final accuracy, whereas too large or too small learning rates tend to degrade performance. Weight tying setting does not affect model performance.

We emphasize that each ablation in Table 4 varies only a single hyperparameter at a time, keeping all other settings identical to our main experiment. In practice, these hyperparameters interact in a coupled manner. For instance, with a smaller learning rate of  $5 \times 10^{-5}$ , we can extend the first-stage training to 300 epochs and get 97.0% accuracy. For deeper models with  $L = 12$ , prolonging first-stage training to 400 epochs and reducing the learning rate to  $5 \times 10^{-5}$  improves accuracy to 99.6%. A comprehensive hyperparameter interaction study is beyond the scope of this work and is left for future investigation.

## F.2 MULTI-LAYER TRANSFORMERS AND MECHANISTIC PATTERNS

We use the COCONUT model with  $L = 4$  to analyze the reasoning pattern beyond two-layer transformers. The results are shown in Figure 7 and Figure 8, and we summarize the reasoning patterns below.

- **First layer (induction head):** The first layer performs token-level copying, propagating node information into edge tokens  $<e>$ , consistent with the copy mechanism derived in previous theoretical analysis (Zhu et al., 2025).
- **Second layer and beyond (superposition):** From the second layer onward, the model aggregates over reachable nodes in a superpositional representation that enables parallel breadth-first exploration.

## F.3 ACCURACY DYNAMICS IN THE ANSWER-PREDICTION STAGE

We track the test accuracy during the final answer-prediction stage following the setting in Figure 4. The result is shown in Figure 9, which shows a rapid transition from near-random guessing to stable high accuracy once the model integrates residual carryover and candidate lift signals.

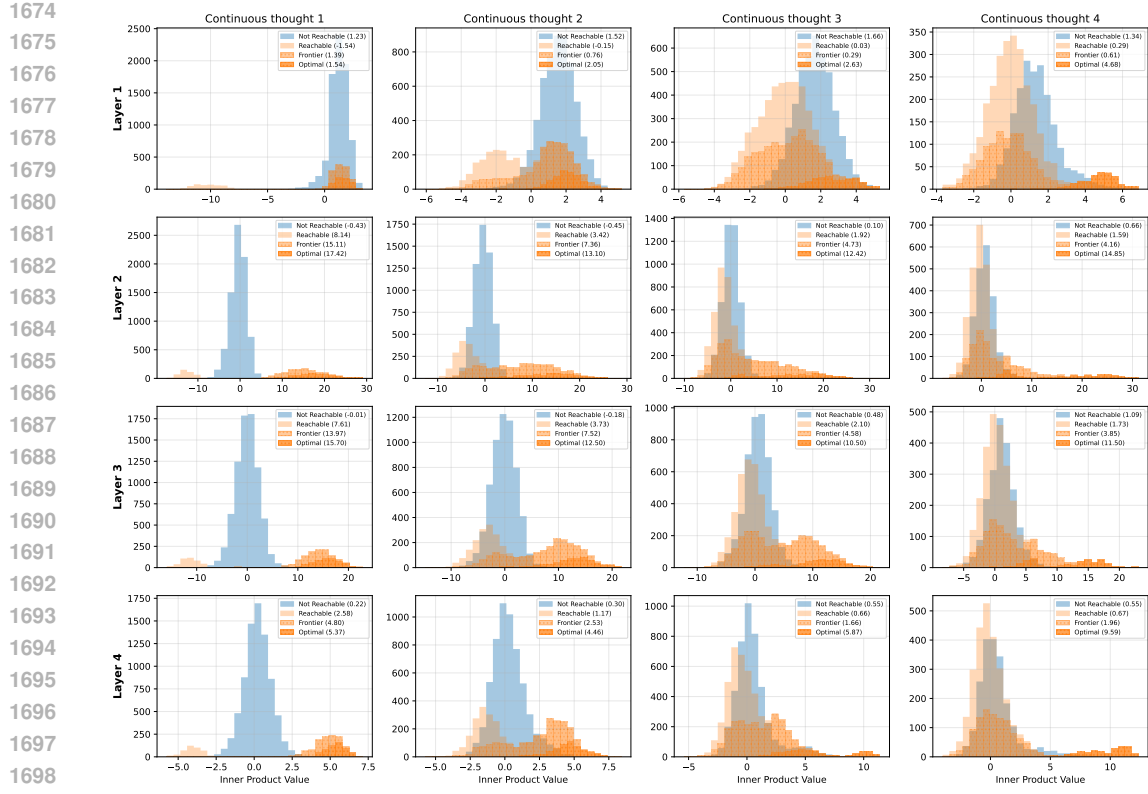


Figure 8: Inner product between layer-wise hidden states and different types of nodes in a 4-layer transformer. The experimental setting follows Zhu et al. (2025). From the second layer onward, hidden states exhibit larger inner products with reachable, frontier, and optimal nodes, indicating that superpositional representations emerge as early as layer 2 in the 4-layer transformer.

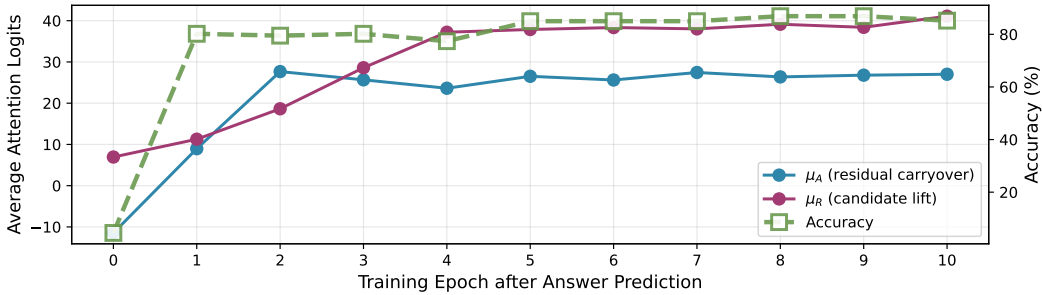


Figure 9: Accuracy curve during the answer-prediction stage. The accuracy shows a rapid improvement corresponding to the learning of residual carryover and candidate lift signals.

## G THE USE OF LARGE LANGUAGE MODELS (LLMs)

We used LLMs mainly for grammar checking and polishing in paper writing.